PART-A

Silicotungstates anchored to MCM-48

Chapter 1

Parent Silicotungstic acid (SiW_{12}) anchored to MCM-48:

Synthesis, Characterization and Esterification as well as Acetalization reactions

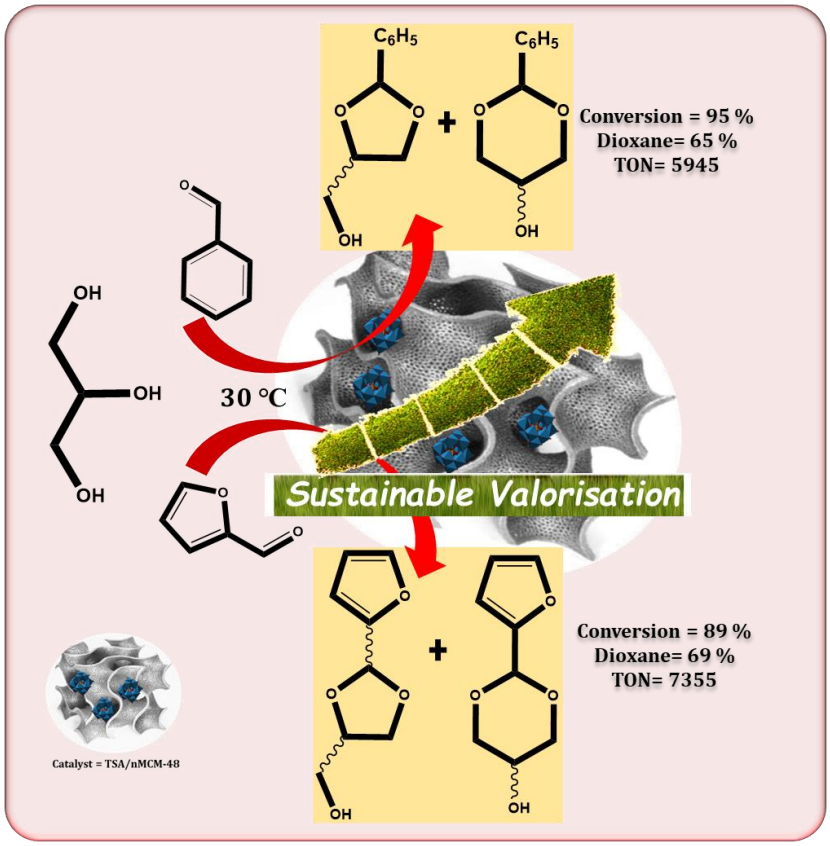

Applied Catalysis A, General 602 (2020) 117729

Contents lists available at ScienceDirect

Applied Catalysis A, General

journal homepage: www.elsevier.com/locate/apcata

Low temperature synthesis of bio-fuel additives via valorisation of glycerol with benzaldehyde as well as furfural over a novel sustainable catalyst, 12-tungstosilicic acid anchored to ordered cubic nano-porous MCM-48

Anjali Patel*, Dhruvi Pithadia

Polyoxometalates and Catalysis Laboratory, Department of Chemistry, Faculty of Science, The Maharaja Sayajirao University of Baroda. Vadodara, 390002, Gujarat, India

ARTICLE INFO

Keywords:
Bio-fuel additives
Glycerol
Valorisation
Acetalization
Heterogeneous catalyst
High TON

ABSTRACT

The present article demonstrates designing of novel catalyst, 12-tungstosilicic acid (TSA) anchored to ordered nano-porous MCM-48 (nMCM-48); TSA/nMCM-48, characterization and evaluation for synthesis of bio-fuel additives via glycerol valorisation with aromatic aldehydes. The nanopores of support were confirmed by BET and TEM while the interaction between TSA and nMCM-48 was confirmed by decrease in the surface area and pore volume of the catalysts. Assessment of vital reaction parameters (% loading of active species, mole ratio of reactants, catalyst amount, temperature and time) were performed to achieve maximum conversion of glycerol. The catalyst showed noteworthy performance at 30 °C towards conversion (> 85 %) and thermodynamically stable dioxane derivative (> 60 %) with remarkable TON (5945 for benzaldehyde and 7355 for furfural). The catalyst was regenerated and used for successive four catalytic runs with almost same activity. The superiority of novel catalyst is because of its geometry and nano porosity.

For the synthesis butyl levulinate via esterification of levulinic acid with n-butanol, in recent times few systems, such as, organic-inorganic hybrid materials [1], modified silica [2–4], mesoporous materials [5–7], enzymes [8,9], titania nanotubes [10,11], carbonaceous solid acid [12], graphene oxide [13], zeolites [14,15], modified clays [16], metal-organic frameworks (MOFs) [17], ion-exchange resins [18] modified [19] as well as supported silicotungstic acid [20] have been reported. In 2016, Gong et al. described the synthesis of butyl levulinate (96.5%), by using an organic salt of 12-tungstosilicic acid and quinaldic acid, at reflux temperature for 5 h [19]. In 2016, Zheng et al. reported the use of 12-tungstosilicic acid immobilized on MCM-41 for butyl levulinate synthesis and obtained approximately 87% conversion at 70 °C in 10 h [20].

Subsequently, for the to synthesize butyl succinates via esterification of succinic acid with n-butanol, number of heterogeneous catalysts, such as DBSA (Dodecylbenzene sulfonic acid), Nafion NR-50, Amberlyst 131, Nafion SAC, Polystyrene sulfonic acid [21], silica-supported acidic ionic liquid [22], Mg^{+2} modified polystyrene sulfonic acid resin [23], lipase immobilized carbon nanotubes [24], halloysite [25], and supported silicotungstic acid [26–28] have been reported. During 2011, Patel et al. reported the synthesis of dibutyl succinate using 12-tungstosilicic acid anchored to MCM-41. They obtained 90% yield of dibutyl succinate at 80 °C in 14h [26].

To synthesis of cyclic acetals via acetalization of glycerol and furfural, heterogeneous catalysts for instance, mesoporous aluminosilicates [29–32], clays [29,32–34], metal oxides [35,36], acidic resin [37], porous organic polymer [38], zeolites [32,39], acidic carbon [40], mesoporous zirconia [41], modified mesoporous MCM-41 [42], TiO_2–ZrO_2 solid acid [43] and coordination polymer [44] have been employed. However, until now, no reports are available for this transformation using POMs based heterogeneous catalysts.

Thus, a literature survey shows that only few reports are available on the utilization of silicotungstates based catalysts for each transformation.

The present chapter deals with the non-hydrothermal synthesis of nano-porous MCM-48 (nMCM-48) support and parent Silicotungstic acid (SiW_{12}) anchored to nMCM-48, SiW_{12}/nMCM-48 (catalyst) by wet impregnation method. A detailed characterization of support as well as catalyst using, acidity measurement, BET surface area measurements, elemental analysis (EDS), TGA, FT-IR, Powder XRD, ^{29}Si MAS NMR and TEM was carried out. The catalytic activity of SiW_{12}/nMCM-48 was evaluated for the esterification of levulinic and succinic acid with n-butanol as well as the acetalization reaction of glycerol with furfural. A detailed optimization study for all the reactions was carried out by varying different reaction parameters, such as mole ratio of reactants, catalyst amount, reaction temperature and time. The regeneration and recycling studies were also carried out along with the characterization of regenerated catalysts. In addition, kinetic experiments were carried out to determine the activation energy of the reactions. lastly, for all transformations their mechanistic pathways were proposed.

EXPERIMENTAL

Materials

All chemicals used were of A.R. grade. Silicotungstic acid, 25 % (w/v) liquor ammonia, tetraethylorthosilicate (TEOS), ethanol, levulinic acid, succinic acid, glycerol, n-butanol, furfural, dichloromethane, methanol and 2-propanol were used as acquired from Merck. CTAB (Cetyltrimethylammonium bromide) was purchased from Loba Chemie.

Synthesis of support, nano-porous MCM-48 (nMCM-48)

The synthesis of nMCM-48 was carried out by the method previously reported by us with some modifications [45]. In 50 mL of distilled water, 2.4 g (6.6 mmol) CTAB surfactant was added and stirred at 35 ˚C to dissolve completely. To this solution, 50 mL (0.87 mmol) ethanol and ~15.4 mL (0.225 mol), 25% (w/v) liquor ammonia were added and allowed to stir for 15-20 min, followed by the dropwise addition of 3.4 g (16 mmol) TEOS. The resulting white suspension was

aged for 2 h, filtered and washed with distilled water. It was dried at room temperature and calcined at 550 ˚C for 6 h. The resulting material was designated as nMCM-48 (Scheme 1).

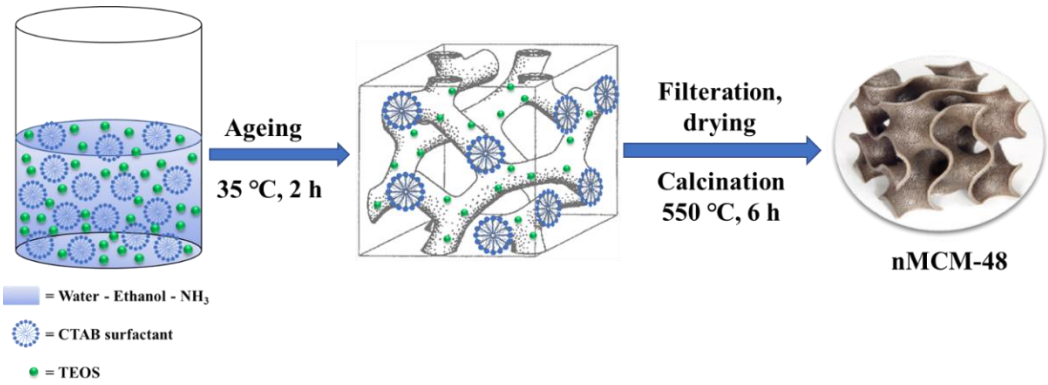

Scheme 1 Synthesis of nMCM-48.

Synthesis of catalyst, silicotungstic acid anchored to nMCM-48 (SiW_{12}/nMCM-48)

A series of catalysts containing 10 - 40% of SiW_{12} anchored to nMCM-48 were synthesized by a wet impregnation method. 1 g of nMCM-48 was suspended in an aqueous solution of SiW_{12} (0.1 g/10 mL – 0.4 g/40 mL of double-distilled water) and dried at 100 ˚C for 10 h (Scheme 2). The obtained catalysts were designated as $(SiW_{12})_1$/nMCM-48, $(SiW_{12})_2$/nMCM-48, $(SiW_{12})_3$/nMCM-48, and $(SiW_{12})_4$/nMCM-48, respectively.

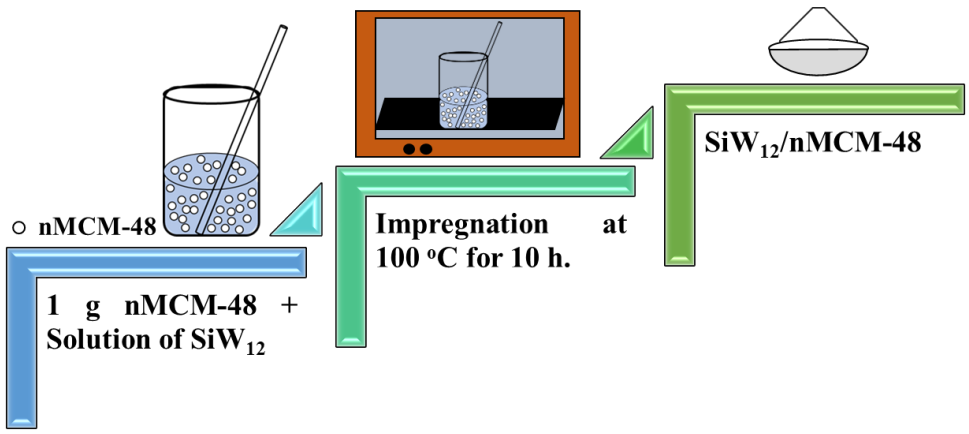

Scheme 2 Synthesis of SiW_{12}/nMCM-48

Characterization

Characterization of nMCM-48 and SiW_{12}/nMCM-48 was carried out by the same physicochemical techniques as mention in General Introduction [Page 41-46].

Catalytic activity

The esterification of levulinic acid and succinic acid, as well as acetalization of glycerol were carried out by the procedure as given in General Introduction [Page 47-59].

RESULTS AND DISCUSSION

Characterization

Acidity measurement

A quantitative measure of the types of acidic sites, as well as the acidic strength of all the catalysts, was determined by the potentiometric titration method. The plots of the electrode potential as a function of mEq n-butylamine per g of the material are shown in Figure 1 the acidic strength in terms of initial electrode potential and the acid sites are presented in Table 1. From the data, it is well distinct that as the loading amount of SiW_{12} on nMCM-48 increases from 10 – 30%, the acidic strength, as well as acid sites, increases significantly. This observed enhancement in the acidity can be attributed to the increase in the concentration of Bronsted acidity present in SiW_{12}. However, a negligible change in the acidic strength and sites was observed from 30 – 40% loading which may be due to the blocking of the sites or insufficient impregnation.

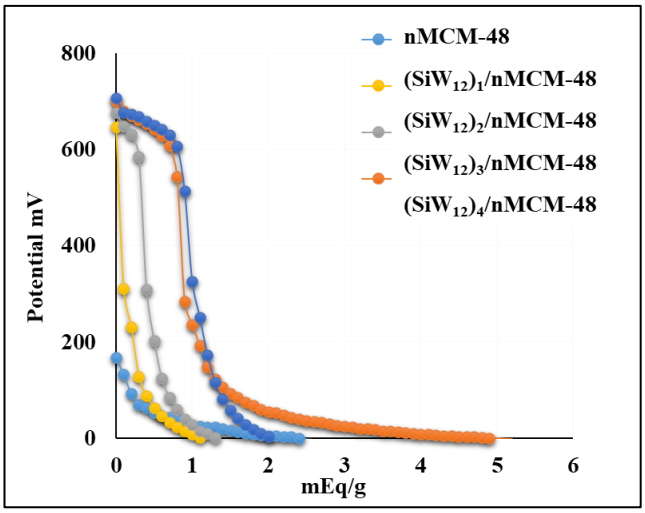

Figure 1 Potentiometric titration curves

Table 1 Acidity measurements of support and catalysts

Materials	Acidic strength (mV)	Types of acidic sites (mEq/g)		Total No. of acidic sites (mEq/g)
		Very strong	Strong	
nMCM-48	168	0.1	2.3	2.4
$(SiW_{12})_1$/nMCM-48	646	0.3	2.3	2.6
$(SiW_{12})_2$/nMCM-48	676	0.6	2.7	3.3
$(SiW_{12})_3$/nMCM-48	700	1.4	3.5	4.9
$(SiW_{12})_4$/nMCM-48	706	1.3	3.6	4.9

BET surface area measurement

The textural properties of nMCM-48 and catalysts are shown in Table 2. The relatively small pore diameter of nMCM-48 gives the first indication that the support is nano-porous with a high specific surface area. A significant decrease in both, the surface area as well as pore volume with the increase in the loading amount of SiW_{12} indicates its successful impregnation inside the porous network of nMCM-48. Also, it is very interesting to note down that in 40% loading, a decrease in surface area and a slight increase in the pore volume were observed. This may be attributed to the blocking of the sites because of the multilayer adsorption of SiW_{12} as observed in acidity measurement also. Therefore, looking

at the values of acidity measurements as well as textural properties, 30% loading of SiW_{12} was considered to be optimum and $(SiW_{12})_3$/nMCM-48 was selected for detailed characterization and further studies. For simplicity, it is redesignated as SiW_{12}/nMCM-48.

Table 2 Textural properties of support and catalysts

Materials	BET Surface area (m^2/g)	Pore diameter (Å)	Pore volume (cm^3/g)
nMCM-48	1307	20.8	0.63
$(SiW_{12})_1$/nMCM-48	712	20.1	0.24
$(SiW_{12})_2$/nMCM-48	637	19.2	0.25
$(SiW_{12})_3$/nMCM-48	588	18.3	0.21
$(SiW_{12})_4$/nMCM-48	333	17.8	0.23

The Nitrogen adsorption-desorption isotherms of nMCM-48 and SiW_{12}/nMCM-48 are shown in Figure 2. Both the isotherms are of the typical nature of type IV(b), confirming the formation of mesoporous structure. According to the IUPAC technical report, the capillary condensation occurring in the pores having smaller widths is completely reversible and in the absence of a hysteresis loop. In the present case, completely reversible isotherms are obtained without a hysteresis loop, indicating the smaller width and confirming the nano-porous structure. The observation is in good accord with the reported one [46]. The uniformity in the size of nanopores is well distinct from the position of the inflection point which is related to the diameter of pores and the sharpness of the step. In the case of nMCM-48, the adsorption in the mesopores is well distinct in the range of relative pressure between 0.2 - 0.3, which disappears for SiW_{12}/nMCM-48, indicating the effective filling of mesopores by SiW_{12} [47].

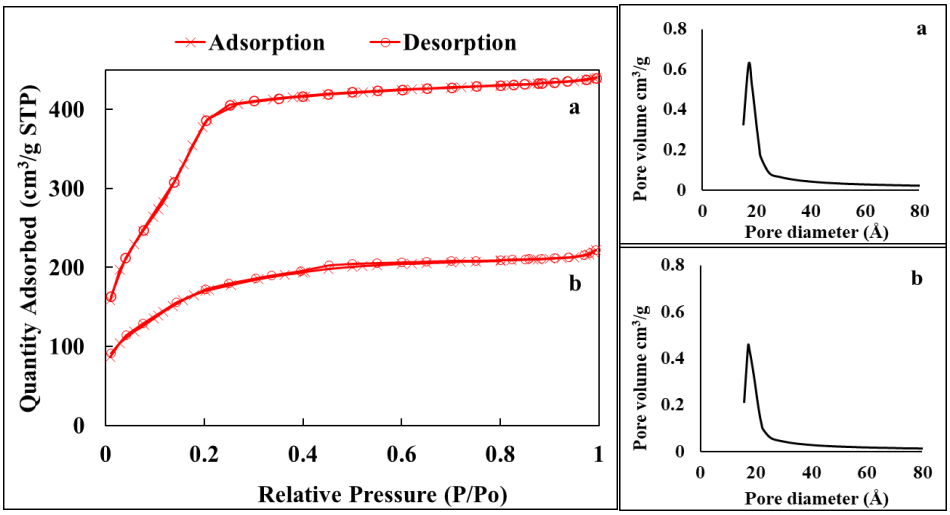

Figure 2 Nitrogen adsorption-desorption isotherms and pore size distribution of a) nMCM-48 and b) SiW_{12}/nMCM-48

Elemental analysis

The EDS elemental analysis and mapping for SiW_{12}/nMCM-48 are shown in Table 3 and Figure 3, respectively. The mapping shows the presence of all expected elements, and the results obtained for W wt% are in good agreement with that of the theoretically calculated value.

Table 3 Elemental analysis of catalyst

Material	Si (wt%)	O (wt%)	W (wt%)	
			By EDS	Theoretical
SiW_{12}/nMCM-48	23.73	58.93	17.34	17.7

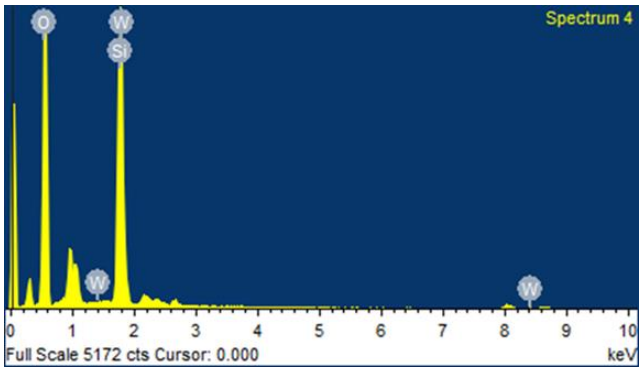

Figure 3 EDS elemental mapping of SiW_{12}/nMCM-48

TGA

The TGA curves for nMCM-48 and SiW_{12}/nMCM-48 are shown in Figure 4. the curves show that the weight loss occurs mainly in two stages. For nMCM-48, the initial weight loss of 8.9% was observed up to 110 °C, which may be due to the desorption of physically absorbed water molecules. The final weight loss of <1 % up to 400 °C can be attributed to the condensation of silanol groups present in the nMCM-48 [45]. No further weight loss was observed, which indicates the stability of support up to 550 °C. In the case of SiW_{12}/nMCM-48, the initial weight loss of 8.1% up to 115 °C corresponds to adsorbed water molecules. The second weight loss of 0.67% up to 200 °C can be attributed to crystalline water molecules present in the Keggin unit [48]. After that, no gradual weight loss was observed up to 550 °C, indicating the stability of the catalyst.

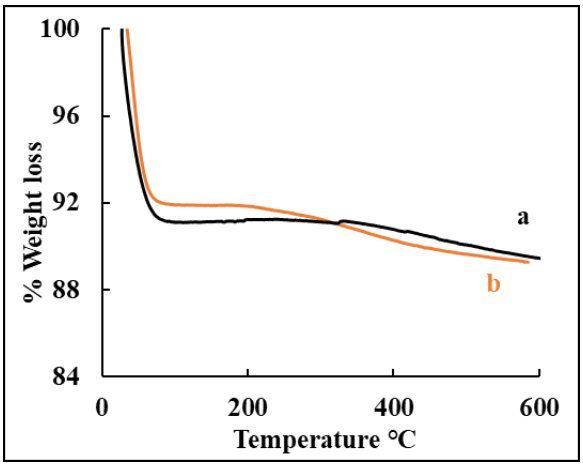

Figure 4 TGA curves of a) nMCM-48 and b) SiW_{12}/nMCM-48

FT-IR

The FT-IR spectrum (Figure 5) of pure nMCM-48 shows a broad band at 1100 cm^{-1} - 1250 cm^{-1} corresponding to Si-O-Si asymmetric stretching. The bands at 578 and 462 cm^{-1} are attributed to the symmetric stretching of Si-O-Si and bending vibration of Si-O, respectively. A symmetric stretching vibration of Si-O-Si and a bending vibration of Si-O are represented by the bands around 578

and 462 cm^{-1} respectively. The broad band at 3448 cm^{-1} is due to the absorption of the hydroxyl group present in silanol groups as well as water molecules. The obtained bands are in good agreement with the reported ones [49]. The FT-IR spectrum of SiW_{12}/nMCM-48 shows two characteristic bands for the Keggin unit at 972 and 925 cm^{-1} corresponding to asymmetric vibrations of W-O_d (terminal oxygen linked to a lone tungsten atom) and Si-Oa respectively. The presence of these bands in the fingerprint region indicates that the primary structure of SiW_{12} remains unchanged even after impregnation on the support. The non-appearance of other characteristic bands, around 880 cm^{-1} (Vas (W-Ob-W)) and 785 cm^{-1} (Vas (W-Oc-W)) of SiW_{12} may be due to their superimposition with the bands of nMCM-48 [50]. Further, an increase in the intensity of the band at 1635 cm^{-1} was observed which may be due to the bending vibration of bridging hydroxyl groups, resulting from the hydrogen bond between the terminal oxygen atom of SiW_{12} and hydrogen atom of silanol groups of nMCM-48.

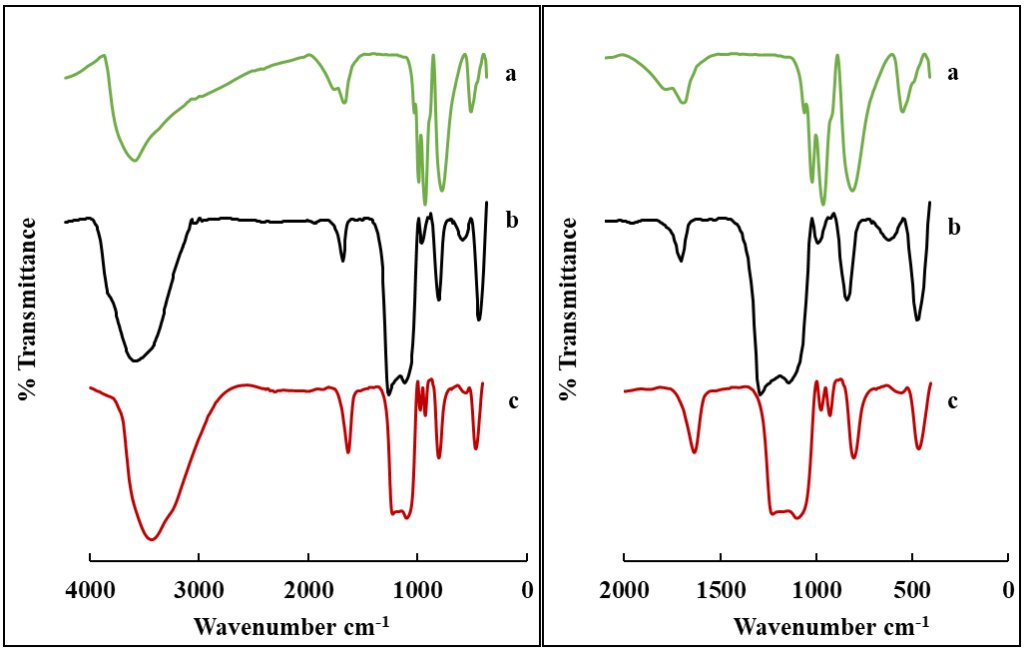

Figure 5 FT-IR spectra of a) SiW_{12}, b) nMCM-48 and c) SiW_{12}/nMCM-48

Powder XRD

The Low-angle and Wide-angle powder XRD patterns for nMCM-48 and SiW_{12}/nMCM-48 are shown in Figure 6. nMCM-48 shows a typical pattern, exhibiting characteristic diffraction peaks at 3.0º and 3.36º 2θ corresponding to the planes 211 and 220, respectively. In the range of 4 – 5º 2θ, numerous peaks corresponding to the reflection planes 400, 321 and 420 of MCM-48 were observed confirming the Ia3d cubic symmetry [51]. The XRD pattern of SiW_{12}/nMCM-48 depicts the decrease in intensity of the characteristic peak with slight broadening which is in good agreement with the reported one [52]. In the Wide angle XRD pattern of SiW_{12}/nMCM-48, the absence of characteristic peaks of the crystalline phase of SiW_{12} signifies its fine dispersion into the pores of nMCM-48 [53]. Collectively, it can be inferred from the XRD results, that the structure of nMCM-48 remains intact even after the impregnation of SiW_{12}.

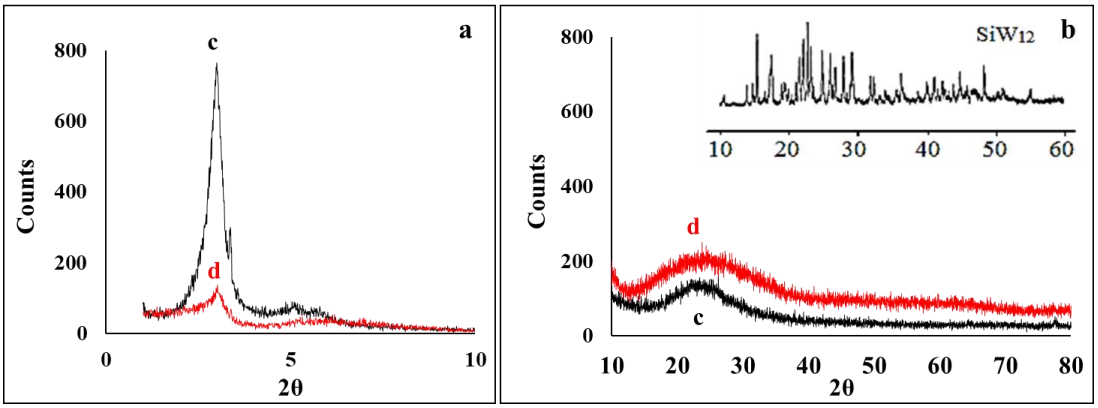

Figure 6 a) Low angle and b) wide angle Powder XRD patterns of c) nMCM-48, d) SiW_{12}/nMCM-48 and SiW_{12} (Inset)

^{29}Si MAS NMR

Solid state ^{29}Si MAS NMR was performed to identify the interactions between nMCM-48 and SiW_{12}. The obtained spectra are depicted in Figure 7. A broad peak for nMCM-48 was observed between -95 and -120 ppm corresponding to the three main signals Q^2, Q^3 and Q^4. The notation Q^x describes the number of x siloxane linkages to a silicon atom. The Q^2 signal corresponds to the disilanol

linkage Si-(O-Si)2 $(-O-X)^{2-}$, where X is H or SiW_{12}. Similarly, Q^3 and Q^4 correspond to the resonating peaks for $(O-X)-Si-(O-Si)_3$ and $Si-(O-Si)_4$, respectively. The chemical shift values for all components are cited in Table 4. The observed chemical shift values for nMCM-48 are in good accord with the reported literature [54]. A downfield shift in the values of chemical shift for all components as well as broadening in the spectrum of SiW_{12}/nMCM-48 was observed as compared to nMCM-48, which may be due to the presence of SiW_{12} in the surrounding environment. Also, a slight change in the intensities of Q^2 and Q^3 peaks was observed, indicating the hydrogen bonding between terminal oxygen of SiW_{12} with the proton of silanol groups of nMCM-48. The signal for SiW_{12} appears in the range of -81 to -90 ppm, which is reflected in the spectrum at -87.97 ppm, showcasing the unchanged Keggin structure of SiW_{12} [55].

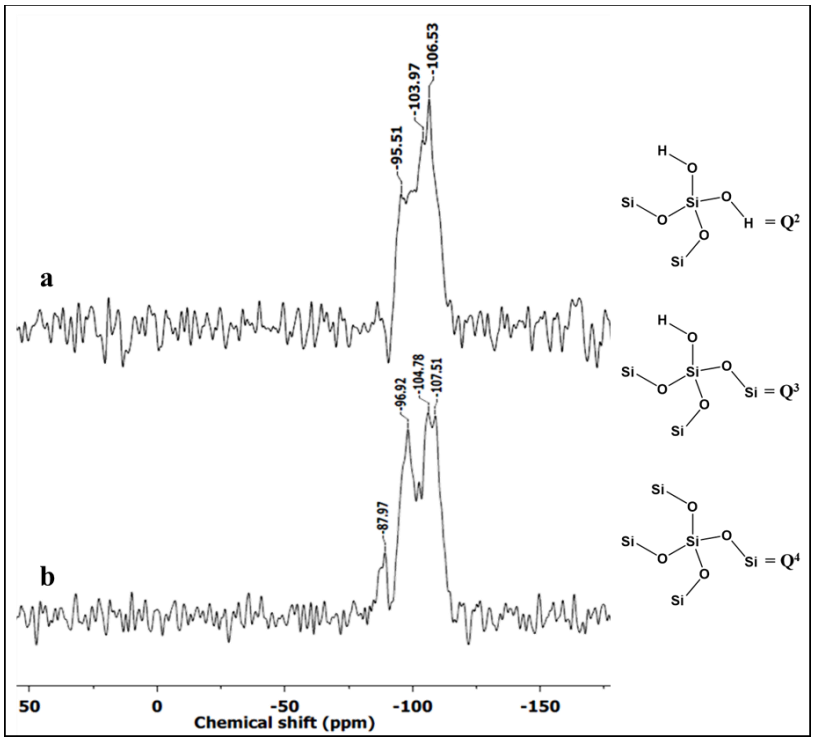

Figure 7 ^{29}Si MAS NMR of a) nMCM-48 and b) SiW_{12}/nMCM-48

Table 4 ^{29}Si chemical shifts of nMCM-48 and SiW_{12}/nMCM-48

Materials	Si nuclei ppm (SiW_{12})	Q^2 ppm	Q^3 ppm	Q^4 ppm
nMCM-48	-	-95.51	-103.97	-106.53
SiW_{12}/nMCM-48	-87.97	-96.92	-104.78	-107.51

TEM

The TEM images of nMCM-48 and SiW_{12}/nMCM-48 were recorded at different magnifications and are shown in Figure 8. nMCM-48 shows well-ordered pore networks with uniform particle diameter, confirming the nano-porous structure, which is in good agreement with the BET surface area analysis. Opaque spheres were observed in SiW_{12}/nMCM-48 (Figure 8c & d), where the maximum pores are uniformly filled with SiW_{12}.

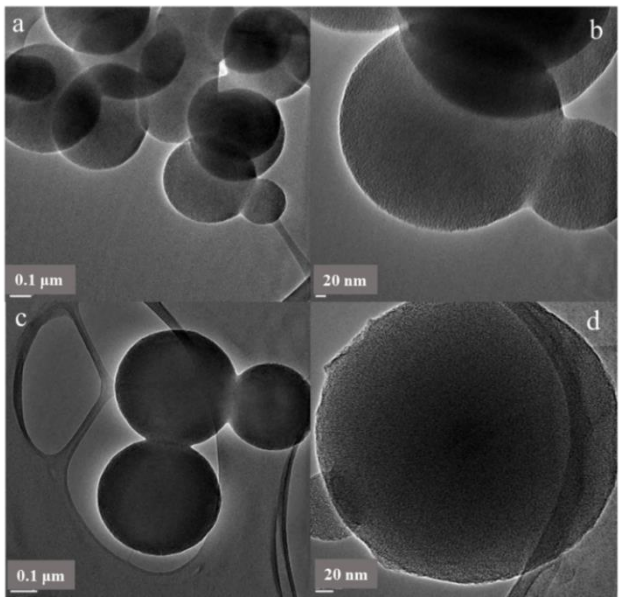

Figure 8 TEM images of a, b) nMCM-48 and c, d) SiW_{12}/nMCM-48

In summary, acidity measurements show an increase in acidic strength and sites after the introduction of SiW_{12} into nMCM-48. The BET surface area indicates successful filling of SiW_{12} into the nanopores of nMCM-48 and FT-IR studies show the unaltered structure of nMCM-48 as well as SiW_{12} after anchoring. TEM, XRD and ^{29}Si MAS NMR confirm the mesostructure with nanopores, fine dispersion of SiW_{12} and hydrogen bonding between SiW_{12} and nMCM-48, respectively.

Catalytic activity

Leaching test

Escape of any active species from the support makes the catalyst unappealing and hence it is mandatory to analyse leaching of SiW_{12} from nMCM-48. Leaching test for SiW_{12}/nMCM-48 was carried out by the method given in General introduction [Page 46]. The absence of heteropoly blue colour indicates no leaching of SiW_{12} from the support nMCM-48. The study indicates the presence of strong interaction between them as well as stability of the catalyst.

a) Esterification of levulinic acid with n-butanol

The catalytic activity of the catalyst was assessed by carrying out the esterification of levulinic acid with n-butanol to synthesize butyl levulinate (Scheme 3). The effect of different reaction parameters for instance, % loading of SiW_{12}, levulinic acid: n-butanol molar ratio, catalyst amount, reaction temperature and time were studied in detail to optimize the conditions for maximum conversion of acid and selectivity of butyl levulinate. (The other product could be psuedobutyl levulinate, an intermediate in the formation of butyl levulinate from levulinic acid [16].)

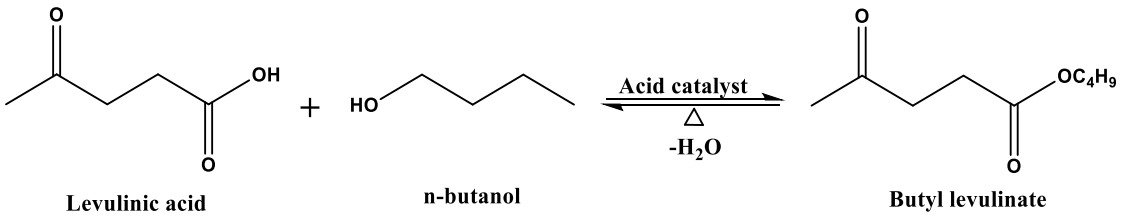

Scheme 3 Esterification of levulinic acid with n-butanol

Primarily, from the viewpoint of catalytic activity, it is important to identify appropriate catalyst loading. The experiments with different % loading of SiW_{12} (10 – 40%) were carried out and the results are shown in Figure 9a. It was observed that the reaction proceeds in a forward direction as the amount of active catalytic acid sites increases with the % loading. From 10 – 30% loading,

the conversion of acid hiked from 56% to 95%. A further increase in the concentration to 40% does not show any significant increase in the conversion. This steady activity at higher concentrations may be attributed to the limitations of mass transfer and/or blocking of the sites due to viscous reaction mixture [56]. This consistent behaviour may be interrelated with the surface area and acidity measurements of 30 and 40% loaded nMCM-48. Therefore, from the above experiments, 30% loading of SiW_{12} was considered appropriate for carrying out further catalytic reactions from the viewpoint of catalytic activity.

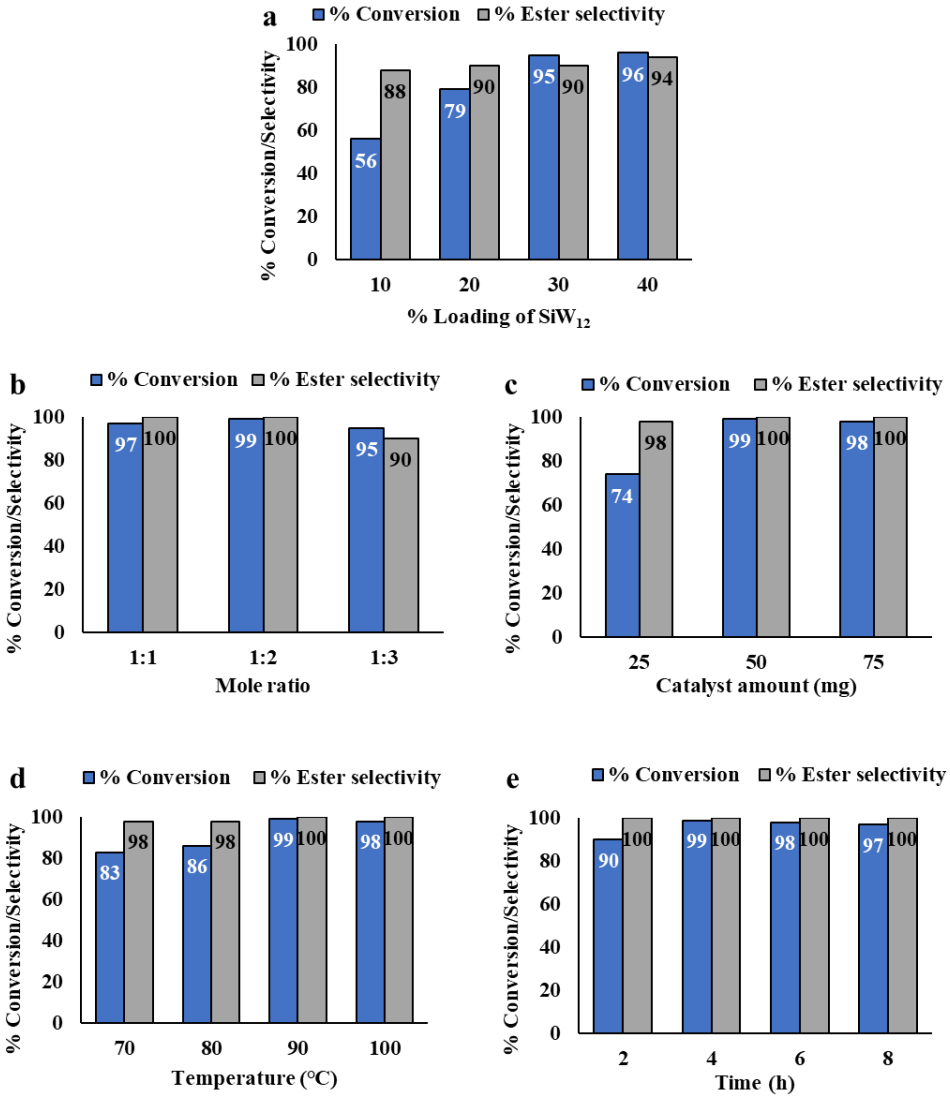

Figure 9 Reaction conditions: a) Effect of % loading of SiW_{12}: Mole ratio: 1:3; Catalyst amount: 50 mg; Temperature: 90 °C; Time: 4 h b) Effect of mole ratio. Catalyst amount 50 mg; Temperature 90 °C; Time 4h, c) Effect of catalyst amount. Mole ratio 1:2; Temperature 90 °C; Time 4h, d) Effect of temperature. Mole ratio 1:2; Catalyst amount 50 mg; Time 4h, e) Effect of time. Mole ratio 1:2; Catalyst amount 50 mg; Temperature 90 °C.

To achieve the best selectivity of the desired product and to limit the side reactions, it is inevitable to study the effect of the mole ratio of reactants. Levulinic acid: alcohol mole ratio was varied from 1:1 to 1:3 and the results are plotted in Figure 9b. Initially, with the increase in a mole ratio from 1:1 to 1:2, the conversion of acid increases. As esterification reaction is a reversible reaction, a slight excess of alcohol shifts the equilibrium in the forward direction and prevents reverse hydrolysis. Consequently, in a 1:2 mole ratio, an excess alcohol component increases the reaction rate. However, when the rate increases to 1:3, the conversion of acid drops slightly, which is probably due to the dilution of the reaction medium and active catalytic sites. Thus, the 1:2 mole ratio was considered to be optimum and applied for further catalytic experiments.

To check the effect of catalyst amount, experiments were carried out using 25 to 75 mg of catalyst and keeping the other parameters constant (Figure 9c). The conversion rate of acid increases from 74 to 99% in 25 to 50 mg of catalyst respectively. As the amount increased to double, the availability of more acid sites favours the conversion of acid and yields 100% selectivity of butyl levulinate. Nonetheless, beyond that, the increase in the amount to 75 mg did not show any significant impact on the conversion. The observed behaviour may be due to the blocking of sites/saturation of the number of active sites available vs. reactant amount. Therefore, a 50 mg catalyst amount was found to be ideal.

Reaction temperature holds enormous importance for the endothermic reactions which shift the equilibrium in a forward direction. The effect of temperature was studied by carrying out reactions in a range from 70 to 100 °C and the results are plotted in Figure 9d. as the temperature exceeds the rate of reaction increases appreciably from 83 to 99%. As the trend observed, an increase in the reaction temperature promotes the reaction rate because of the upsurge in the collisions between reactant molecules. A maximum conversion of 99% was obtained at 90 °C and it was considered to be the optimum temperature. From the viewpoint of

an energy-demanding process, the catalyst works effectively at less than 100 °C temperature.

The effect of reaction time was examined by performing experiments for different time intervals (2 to 8 h) and the results are shown in Figure 9e. Initially, in 2 h 90% conversion was obtained. The conversion increases tremendously to 99% in 4 h. However, when the reaction was prolonged to 6 and 8 h, the conversion slightly declines which may be due to the reverse hydrolysis of ester occurring in the presence of water molecules generated during the reaction. As a consequence, 4 h was considered an appropriate reaction time.

From the above studies, the obtained optimized reaction conditions for maximum conversion of levulinic acid (99%) and selectivity of ester (100%) are, mole ratio (levulinic acid: n-butanol) 1:2; catalyst amount 50 mg (active amount of SiW_{12} 11.54 mg); temperature 90 °C; time 4h with TON 2469 and TOF of 617 h^{-1}.

b) Esterification of succinic acid with n-butanol

Esterification reaction between succinic acid and n-butanol using an acid catalyst yields two ester products- monobutyl succinate (monoester) and dibutyl succinate (diester). The catalytic transformation is shown in Scheme 4. The effect of each reaction parameter was studied by carrying out experiments for varying % loading of SiW_{12}, a mole ratio of succinic acid: n-butanol, catalyst amount, temperature and contact time of reactants for obtaining the maximum conversion of acid. As mentioned earlier the importance of dibutyl succinate, as a fuel additive, in the introduction, the parameters were optimized to yield utmost selectivity towards diester.

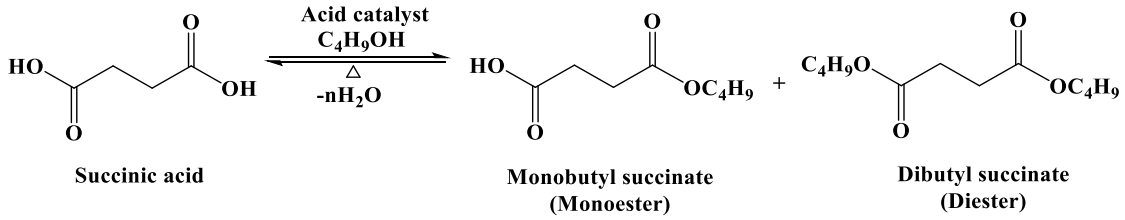

Scheme 4 Esterification of succinic acid with n-butanol

By changing the loading amount of SiW_{12} from 10% to 40%, the reaction proceeds expectedly from 51% to 98% conversion (Figure 10a). As the amount of SiW_{12} increases, the active sites i.e., the Bronsted acidity in the catalyst increases and hence the reaction proceeds forward to yield an appreciable amount of esters. Besides, with more measures of Bronsted acidity from 10 to 40%, the selectivity for the formation of the desired diester also increased from 15% to 85%. However, almost similar results in terms of acid conversion as well as selectivity of diester were observed for the 30% and 40% loaded catalysts. This observation well supports the acidity measurement values, and hence here also, a 30% loading amount of SiW_{12} was considered to be appropriate and all further experiments were carried out using this catalyst.

The mole ratio of acid to alcohol was screened from 1:2 to 1:4 and the obtained results are presented in Figure 10b. A slight excess of alcohol is a boon to the reversible esterification reaction. With the increase in the ratio from 1:2 to 1:3, the reaction proceeds in a forward direction to yield 92% to 98% conversion with a good hike in the selectivity of the diester from 71% to 84%. But, when the ratio was increased to 1:4, the selectivity dropped to 58% and conversion remains almost the same. This decrease in the formation of diester may be attributed to the dilution of a medium by excess alcohol and thus, a less feasible factor for the second esterification step. Henceforth, the 1:3 molar ratio was considered optimum for the reaction.

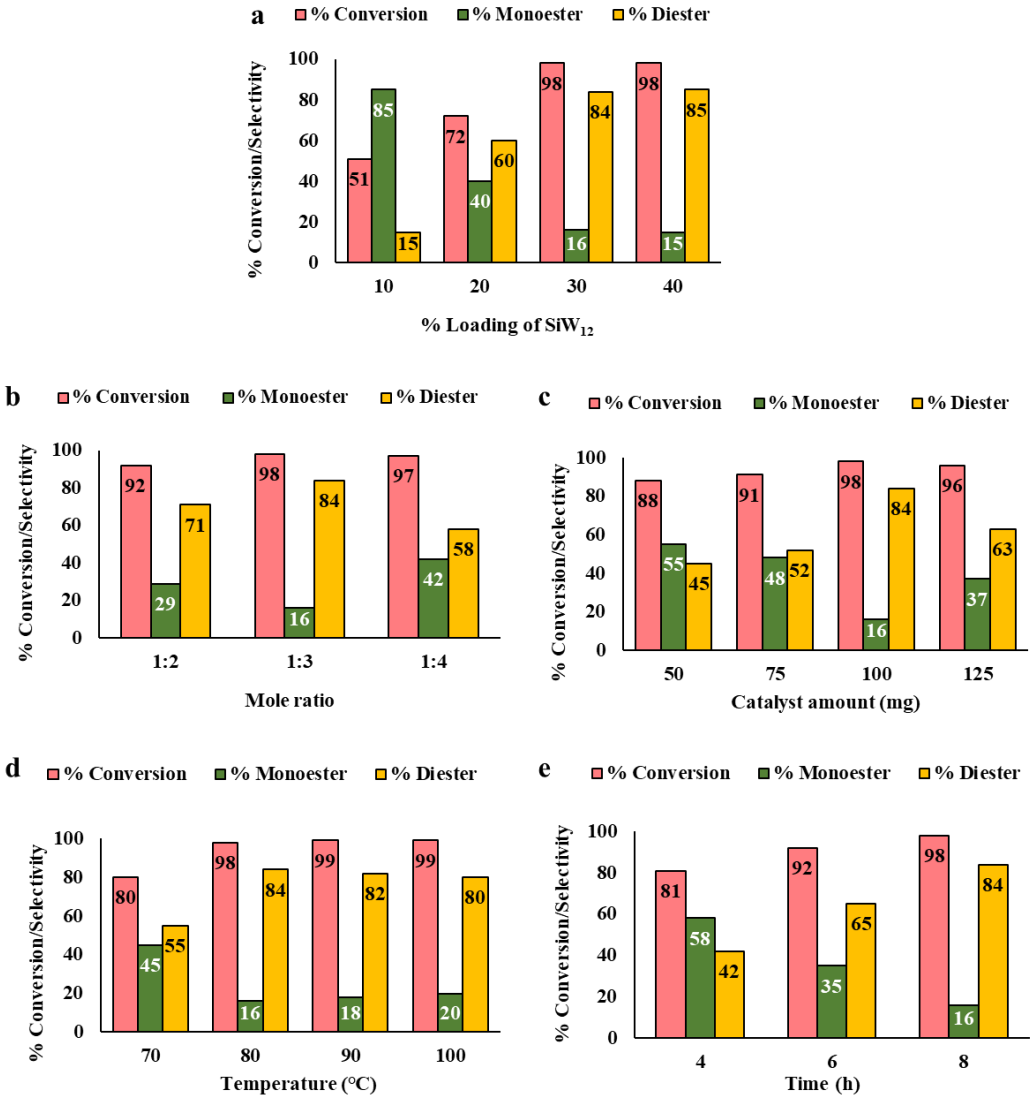

Figure 10 Reaction conditions: a) Effect of % loading of SiW_{12}: Mole ratio: 1:3; catalyst amount: 100 mg; temperature: 80 °C; time: 8 h, b) Effect of mole ratio. Catalyst amount 100 mg; Temperature 80°C; Time 8h, c) Effect of catalyst amount. Mole ratio 1:3; Temperature 80°C; Time 8h, d) Effect of temperature. Mole ratio 1:3; Catalyst amount 100 mg; Time 8h, e) Effect of time. Mole ratio 1:3; Catalyst amount 100 mg; Temperature 80°C.

The effect of the amount of catalyst was studied by performing reactions using 50 to 125 mg catalyst (Figure 10c). Primarily, as the availability of acidic sites increases from 50 mg to 100 mg, the conversion increases gradually from 88 to 98% and diester selectivity from 45 to 84%. Nevertheless, it was observed that with further raise of an amount to 125 mg, the conversion slightly drops (96%), with a major decline in the selectivity of the diester (63%). This observed behaviour of the catalyst may be ascribed to the increase in the solid mass

density of the reaction mixture which may block the active catalytic sites and prevents the diesterification reaction. Consequently, 100 mg catalyst was found to be ideal.

One of the parameters, reaction temperature plays a major role in shifting esterification reactions in the forward direction. The effect of temperature was screened from 70 to 100 °C (Figure 10d). As anticipated, with the rise in temperature from 70 to 80 °C, the rate of conversion and diester formation increases significantly from 90 to 98% and 55 to 84% respectively. Yet, beyond it, the conversion and formation of the diester remain almost constant. Excellent results were observed at 80 °C, i.e., in mild conditions and so, it was found to be an optimum temperature for the reaction.

The reaction was allowed to perform at different time intervals to study the effect of the contact time of reactants (Figure 10e). The rate of conversion increases linearly from 74 to 98%, as the reaction time increased from 4 to 8 h. Furthermore, as the reaction proceeds with time, the monoester formed, gets converted to diester giving excellent selectivity in 8 h. A maximum conversion of 98% and diester selectivity of 84% was achieved in 8 h and hence considered to be the required contact time for the reaction.

From the detailed optimization study, the optimum conditions for the catalytic reaction are mole ratio (Succinic acid: n-butanol) 1:3; catalyst amount 100 mg (active amount of SiW_{12} 23 mg); temperature 80 °C and time 8 h. The maximum conversion of 98% and selectivity of diester (84%) were achieved with the TON of 1227 and TOF of 153 h^{-1}.

c) Acetalization of glycerol with furfural

Glycerol acetalization with heterocyclic aldehyde, furfural yields two cyclic acetals, (2-(furan-2-yl)-1,3-dioxolan-4-yl)methanol (1,3-dioxolane) and 2-(furan-2-yl)-1,3-dioxan-5-ol (1,3 dioxane) (Scheme 5). All the reaction parameters were screened and an optimization study was carried out to obtain the highest conversion as well selectivity for a potential fuel additive, 1,3 dioxane.

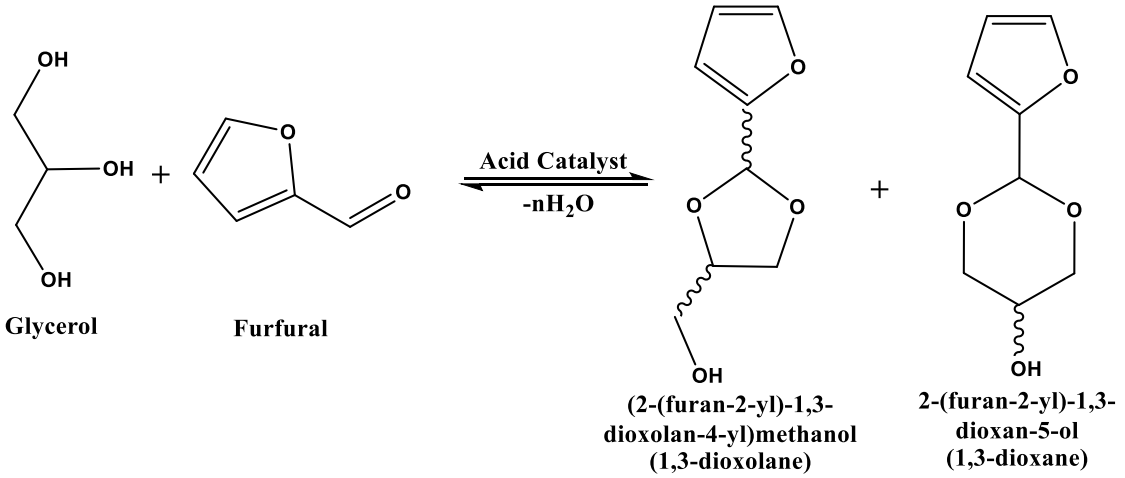

Scheme 5 Acetalization of glycerol with furfural

From Figure 11a, it is observed that as the % loading of SiW_{12} increases, the reaction proceeds to yield 80% acetals with 60% selectivity towards 1,3-dioxane. However, the trend does not show a significant change in activity from 30 to 40 % loading. Hence, considering the equivalent effect as observed for other reactions, here also, the 30% loading amount of SiW_{12} was selected for the detailed study.

The effect of the mole ratio of glycerol to furfural was studied by varying from 1:1 to 1:2 (Figure 11b). 80% glycerol conversion with 60% selectivity of 1,3-dioxane was achieved in a 1:1 mole ratio. By the addition of furfural in double amount (1:2 ratio), a marginal increase in the conversion was observed, however, a decline in the selectivity of 1,3-dioxane was detected. As a result, a 1:1 mole ratio was considered optimum for further catalytic evaluation. The initial feasibility of the catalyst gives an appreciable selective formation of 1,3- dioxane.

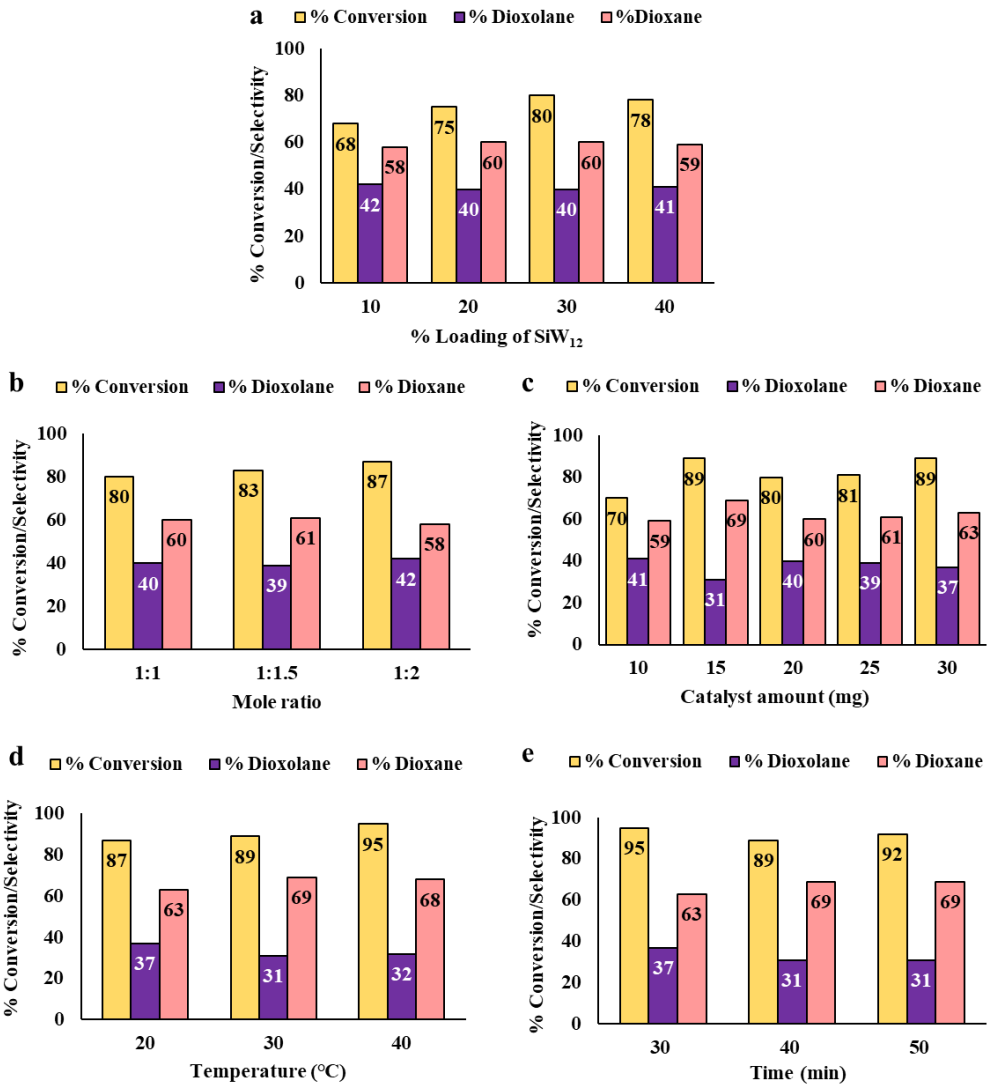

Figure 11 Reaction conditions: a) Effect of % loading of SiW_{12}. Mole ratio 1:1; Catalyst amount 20 mg; Temperature 30 °C; Time 40 min, b) Effect of mole ratio. Catalyst amount 20 mg; Temperature 30°C; Time 40 min, c) Effect of catalyst amount. Mole ratio 1:1; Temperature 30°C; Time 40 min, d) Effect of temperature. Mole ratio 1:1; Catalyst amount 15 mg; Time 40 min, e) Effect of time. Mole ratio 1:1; Catalyst amount 15 mg; Temperature 30°C.

The feasibility reactions for the above two parameters were performed using 20 mg of catalyst amount yielding a good conversion of 80%. Though it is evitable to check the effect in different amounts, the experiments with lower (10 and 15 mg) as well as higher amounts were carried out (Figure 11c). An excellent conversion of 89% with 69% selectivity was achieved in only 15mg of catalyst amount. A further change did not show any significant effect and the observed behaviour may be due to the blocking of sites/saturation of the number of active

sites available vs. reactant amount. Hence, 15 mg was considered to be the optimum amount.

It is well-known that acetalization reaction has a low equilibrium constant and is exothermic [57]. Screening of reaction temperature from 20 to 40 °C was carried out and the results are plotted in Figure 11d. With the temperature rise, the reaction progresses to 95% at 40 °C. But there was no positive effect on the selectivity of desired product relative to that in 30 °C. Hence, an easily accessible temperature, of 30 °C was optimized.

Finally, the reaction time was assessed for 30 to 50 min (Figure 11e). A maximum conversion of 95% was achieved in the 30 min period with 93% selectivity of 1,3-dioxane. Nevertheless, the highest selectivity (69%) was attained in 40 min and prolonging the reaction to 50 min, a negligible rise of 3 % in glycerol conversion was observed which indicates the establishment of equilibrium beyond 40 min. Thus, at the expense of 6% conversion and gain of highest selectivity towards the desired product, 40 min was considered to be the optimum time for reaction.

The optimized reaction conditions for the maximum conversion of glycerol (89%) and selectivity of 1,3-dioxane (69%) are mole ratio (Glycerol: furfural) 1:1; catalyst amount 15 mg (active amount of SiW_{12} 3.5 mg); temperature 30 °C; time 40 min with an outstanding TON 7355 and TOF of 10978 h^{-1}.

The obtained products from all three reactions were analysed by gas chromatography and confirmed by their respective standard samples. The gas chromatographs after the reaction in their respective optimized conditions are shown below in Figure 12, Figure 13 and Figure 14.

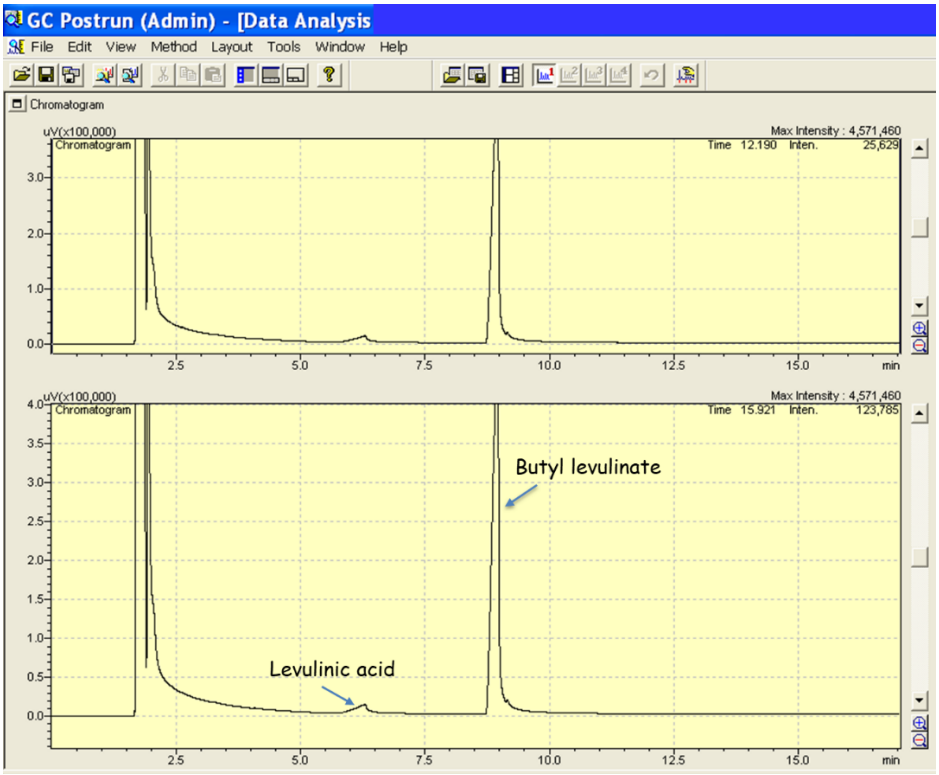

Figure 12 Gas chromatograph of levulinic acid esterification

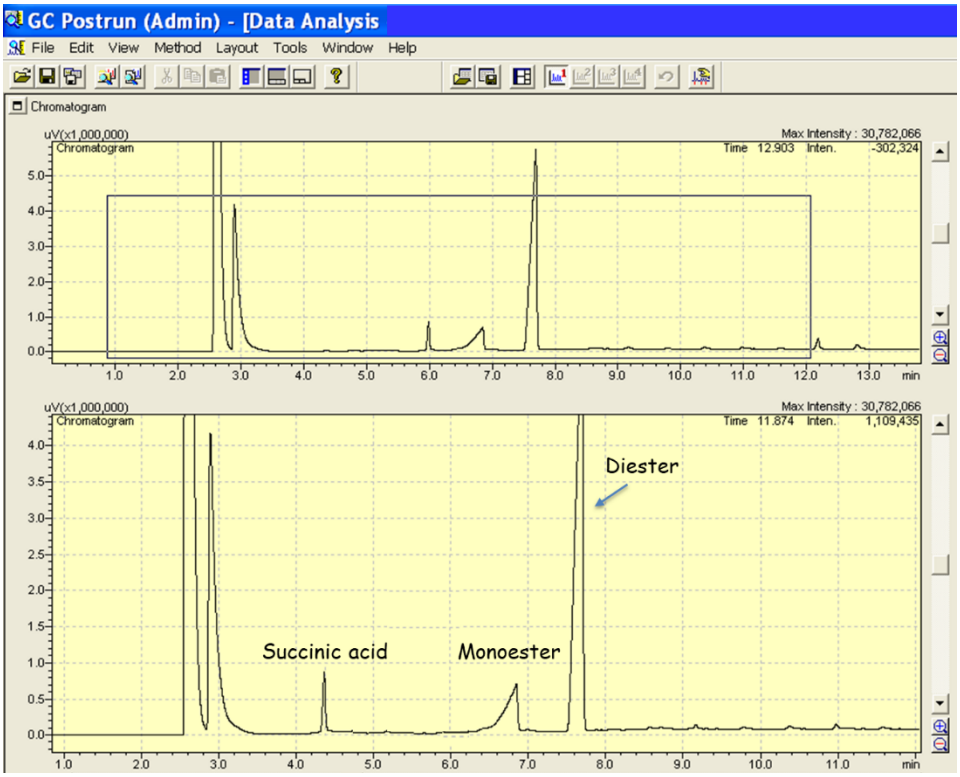

Figure 13 Gas chromatograph of succinic acid esterification

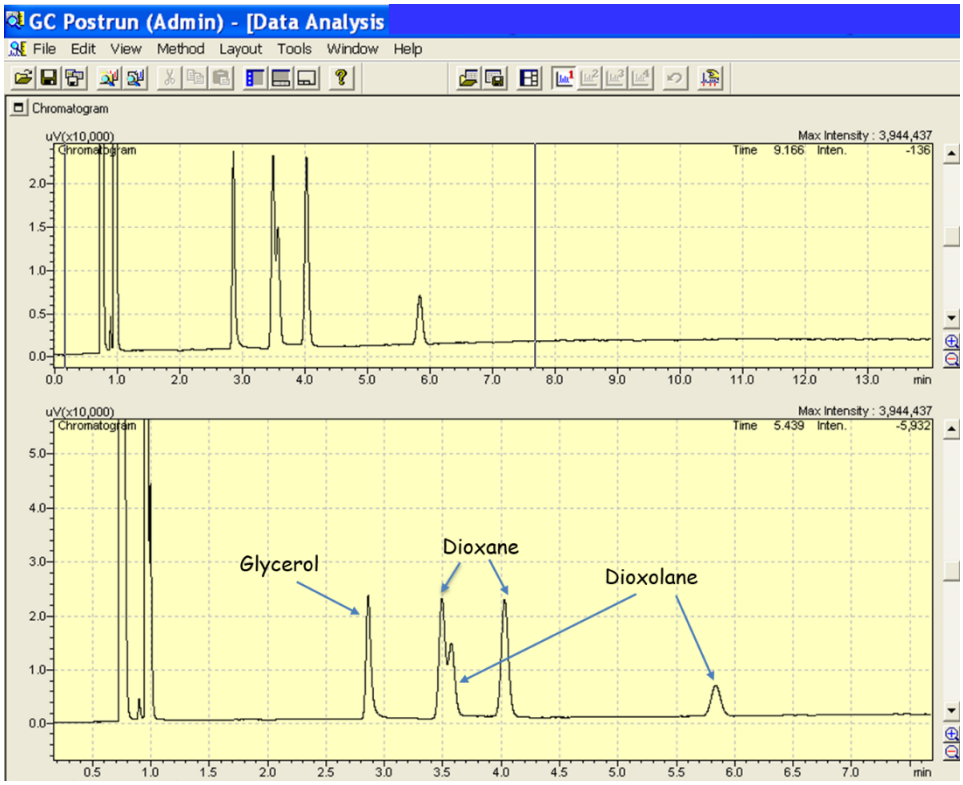

Figure 14 Gas chromatograph of glycerol acetalization

Control experiments

The control experiments for all the reactions were carried out in their respective optimized reaction conditions. From the results demonstrated in Table 5, it was observed that alone nMCM-48 is not active for the anticipated transformations and almost similar catalytic conversion as well as selectivity for the desired products were obtained for SiW_{12} and SiW_{12}/nMCM-48. This confirms that the activity is mainly due to the active keggin unit and suggests that the enhancement of acidic sites by Bronsted acidity present in SiW_{12} plays a significant role in promoting the reaction towards a forward direction. Hence, it can be attributed to the successful anchoring of SiW_{12} and fruitful synthesis of truly heterogeneous catalyst.

Table 5 Control experiments

Materials	% Conversion/% *Selectivity of desired product		
	[a]Levulinic acid esterification	[b]Succinic acid esterification	[c]Glycerol acetalization
nMCM-48	24/100	21/16	3.1/52
SiW_{12}	96/100	100/81	91/58
SiW_{12}/nMCM-48	99/100	98/84	89/69

Reaction conditions mole ratio [a]1:2, [b]1:3, [c]1:1; catalyst amount nMCM-48 [a]38.46 mg, [b] 77 mg, [c]11.54 mg; SiW_{12} [a]11.54 mg, [b]23 mg, [c]3.5 mg; SiW_{12}/nMCM-48 [a]50 mg, [b]100 mg, [c]15 mg; temperature [a]90 °C, [b]80 °C, [c]30 °C; time [a]4 h, [b]8 h, [c]40 min.
*Selectivity of [a]Butyl levulinate, [b]Diester (Dibutyl succinate) and [c]1,3-dioxane

Regeneration and recycling studies

With a viewpoint of the development of a true heterogeneous catalyst, to fetch out its outstanding feasibility, and to reduce the overall cost of production, it is inevitable to determine the unaltered and sustainable nature of the catalyst. In this regard, the recycling studies in all three reactions were performed. After the completion of the reaction, the catalyst was collected by centrifugation method and washed with 2-5 mL methanol to remove the substrate and product remains from the surface, followed by water wash. The catalyst was dried at 100 °C and regenerated for the use of the next catalytic run. Recycling experiments for all the reactions were carried out until noticeable change in catalytic activity, with all catalysts, throughout the thesis.

From the results shown in Figure 15, it is observed that the catalyst shows considerable activity for esterification of levulinic acid, succinic acid and acetalization of glycerol, with nearly no change in the conversion rate and selectivity of desired products up to four catalytic cycles. However, the decreases in conversion after three cycles may be due to the loss of catalyst amount during regeneration process. Depending on chemist's choice the catalyst can further be

used for more cycles until it is completely deactivated. Thus, the catalyst shows stability up to multiple runs and determines the true heterogeneous nature.

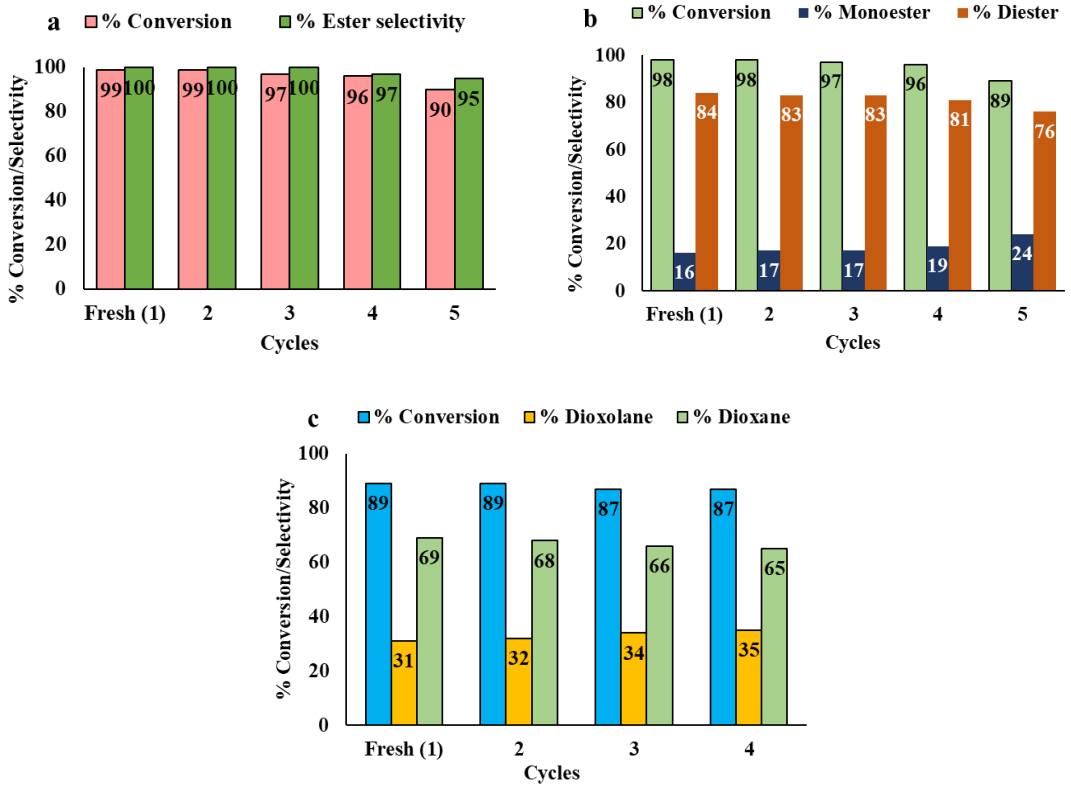

Figure 15 Recycling experiments for a) levulinic acid esterification, b) succinic acid esterification and c) glycerol acetalization

Characterization of regenerated catalyst

The durability and stability of the recycled catalyst were checked by carrying out acidity measurements, BET surface area analysis and FT-IR. The acidic strength and sites obtained by potentiometric titration (Table 6) for regenerated catalyst are found to be in good agreement with that of the fresh one, indicating the unaltered acidic property of the catalyst. The Nitrogen adsorption-desorption isotherms (Figure 16a) of fresh and regenerated catalyst shows indistinguishable isotherms with almost same BET surface area, 588 & 580 m^2/g respectively. This also suggests that there is no degradation in the structure of the catalyst. In FT-IR spectra (Figure 16b), presence of all the characteristic bands with no shifting of values, confirms that there is no leaching of SiW_{12} and change in the structure of catalyst.

Table 6 Acidity measurements and BET surface area of fresh and regenerated catalyst

Catalysts	Acidic strength (mV)	Total acidic Sites (mEq/g)	BET surface area (m^2/g)
Fresh	700	4.9	588
Regenerated	697	4.7	580

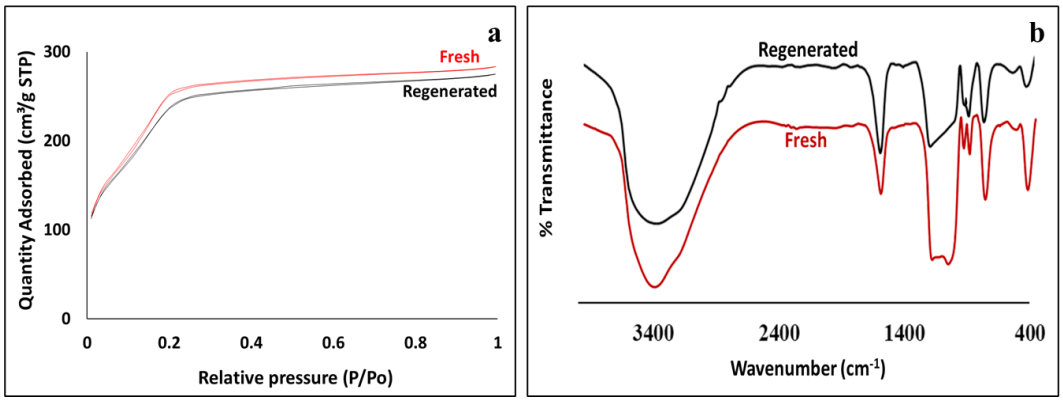

Figure 16 a) Nitrogen adsorption-desorption isotherms and b) FT-IR spectra of regenerated and fresh catalyst

Activity of catalyst for esterification reactions under identical experimental conditions

The activity of catalyst was studied by comparing the esterification of levulinic acid and succinic acid in same conditions and the results are depicted in Table 7. It is seen from the table that in case of succinic acid, less conversion is obtained. It is important to note that levulinic acid is a monocarboxylic keto acid, which requires only one acid group to convert into the desired ester, whereas succinic acid possesses two carboxylic acid groups, a diacid requiring a higher number of catalytic sites as well as prolonged reaction time to undergo diesterification reaction, to obtain the desired diester. Thus, in general, after comparing these experiments, SiW_{12}/nMCM-48 is said to work more efficiently for esterification of a levulinic acid as compared to that of succinic acid, even though there is no major difference in the acidic strength (pKa) of both the acids.

Table 7 Esterification reactions under identical conditions

Conditions / Reactions	In optimized conditions of levulinic acid esterification*	
	% Conversion of acid	% Selectivity of desired ester
Levulinic acid esterification	99	100
Succinic acid esterification	80	56 (Diester)

*Reaction conditions mole ratio 1:2; catalyst amount 50 mg; temperature 90 °C; time 4 h

Kinetic study: Determination of activation energy

To determine the activation energy, four different temperatures were considered for all reactions. For the purpose of comparison studies, the activation energies with other catalysts were also calculated by considering the four temperatures, throughout the thesis.

Kinetic experiments for all the reactions were carried out at different time intervals and varying temperatures, keeping the other parameters the same as in optimized reaction conditions. For all the reactions the rate law is expected to follow second-order dependence.

a) Activation energy for esterification of levulinic acid with n-butanol

Esterification of levulinic acid with n-butanol was carried out with a 1: 2 molar ratio and the reaction mixture was analysed at different time intervals (2, 3 and 4 h) at 80 °C. The plot of 1/(a-x) Vs time (Figure 17) shows a linear relationship with respect to time. This observation confirms the second-order dependence of reaction.

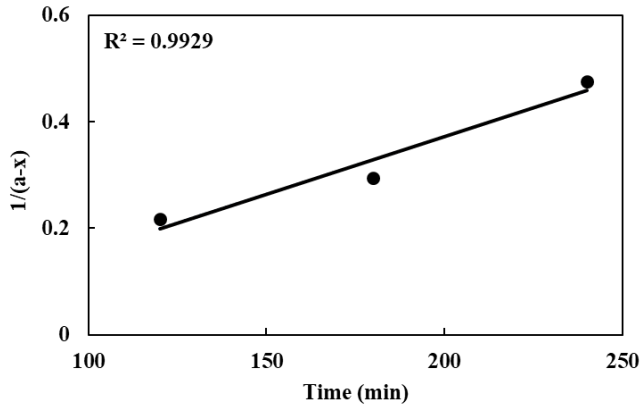

Figure 17 Plot of 1/(a-x) Vs Time for levulinic acid esterification

The rate constant at different temperatures (323 to 353 K) (It should be noted that as the reaction proceeds very fast, giving >90% conversion, at 363 K, the temperature up to 353 K is considered for determining the activation energy.) was calculated (Table 8) and the graph of ln *k* Vs 1/T was plotted (Figure 18). By using the Arrhenius equation, from the slope of the graph, the activation energy was calculated and found to be 26 kJ/mol.

Table 8 Rate constants (*k* M^{-1} min^{-1}) and activation energy (Ea)

Temperature (K)	Rate constant *k* (M^{-1} min^{-1})	Activation energy Ea (kJ/mol)
323	8.5×10^{-4}	26
333	9.0×10^{-4}	
343	1.3×10^{-3}	
353	1.9×10^{-3}	

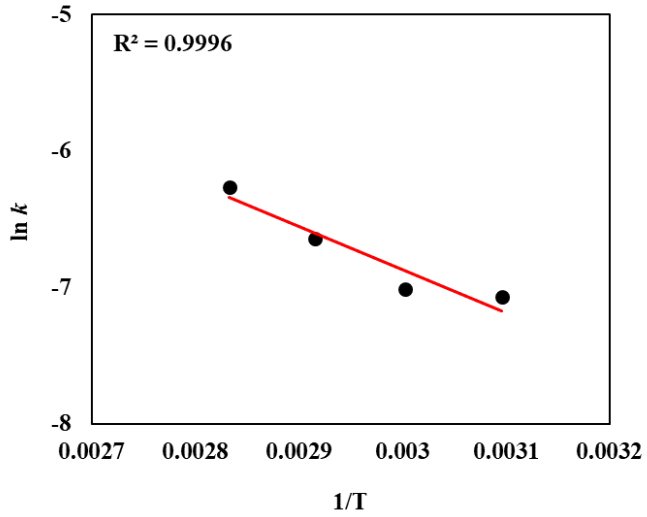

Figure 18 Plot of ln *k* Vs 1/T for levulinic acid esterification

b) Activation energy for esterification of succinic acid with n-butanol

For kinetic experiments, succinic acid and n-butanol were taken in a 1:3 molar ratio and the reaction mixture was analysed at different time intervals (4, 6 and 8 h) at 80 °C. The plot of 1/(a-x) versus time (Figure 19) demonstrates a linear relationship with respect to time and confirms the second-order dependence of reaction.

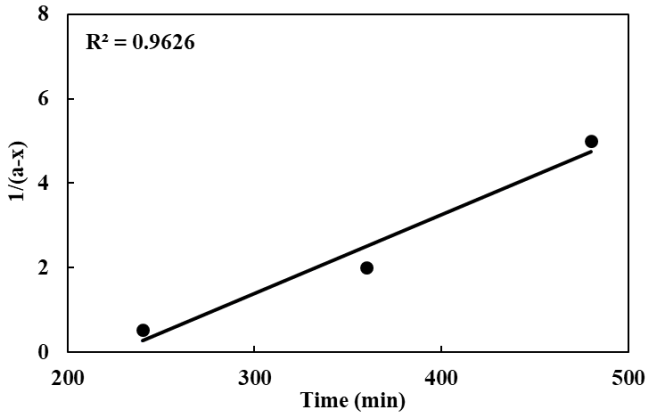

Figure 19 Plot of 1/(a-x) Vs Time for succinic acid esterification

To determine the rate constants, the reactions were carried out in a range of temperatures 343 to 373 K (Table 9). It is observed that the rate constant increases with an increase in temperature and shows a linear relationship. The activation

energy was calculated from the slope of the graph (Figure 20) of ln *k* Vs 1/T using the Arrhenius equation and found to be 55 kJ/mol.

Table 9 Rate constants (*k* M^{-1} min^{-1}) and activation energy (Ea)

Temperature (K)	Rate constant *k* (M^{-1} min^{-1})	Activation energy Ea (kJ/mol)
343	1.21 x 10^{-2}	55
353	1.86 x 10^{-2}	
363	3.57 x 10^{-2}	
373	5.54 x 10^{-2}	

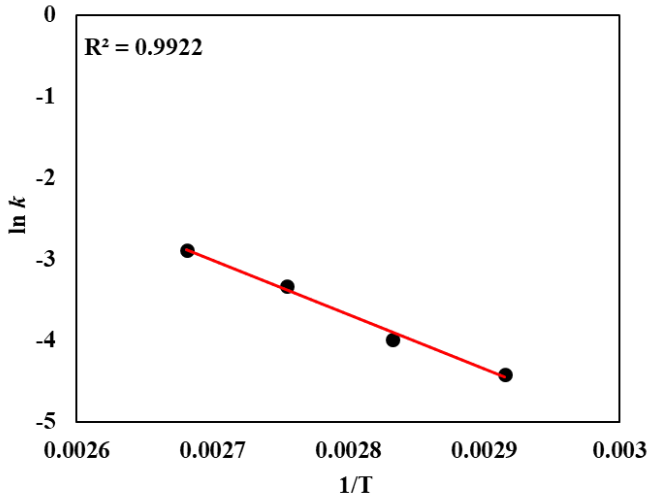

Figure 20 Plot of ln *k* Vs 1/T for succinic acid esterification.

c) Activation energy for acetalization of glycerol with furfural

The kinetic experiments for acetalization of glycerol with furfural were carried out using a 1:1 mole ratio of reactants in different time intervals (20, 40 and 60 min) at 30 °C. The plot of 1/(a-x) Vs time is depicted in Figure 21. It shows the linear relationship, confirming the second-order dependence of reaction.

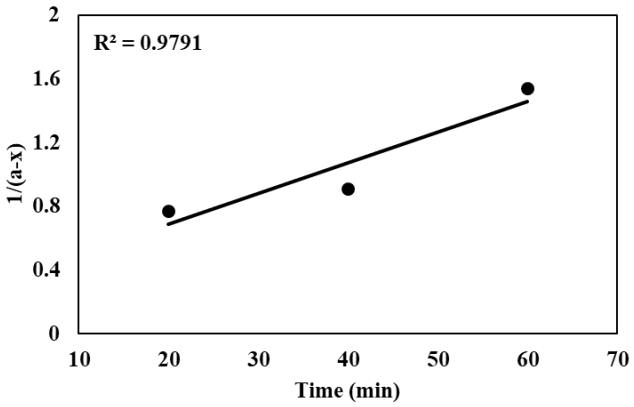

Figure 21 Plot of 1/(a-x) Vs Time for glycerol acetalization

The rate constants at three different temperatures (293 to 323 K) were calculated and the results are mentioned in Table 10. Here also, the rate constants follow the expected trend, as the temperature increases the rate of reaction increases linearly. A graph of ln *k* versus 1/T was plotted (Figure 22) and the activation energy was calculated from the slope of the graph. It was found to be 35 KJ/mol.

Table 10 Rate constants (k M^{-1} min^{-1}) and activation energy (Ea)

Temperature (K)	Rate constant k (M^{-1} min^{-1})	Activation energy Ea (kJ/mol)
293	1.85×10^{-2}	35
303	2.55×10^{-2}	
313	4.73×10^{-2}	
323	6.5×10^{-2}	

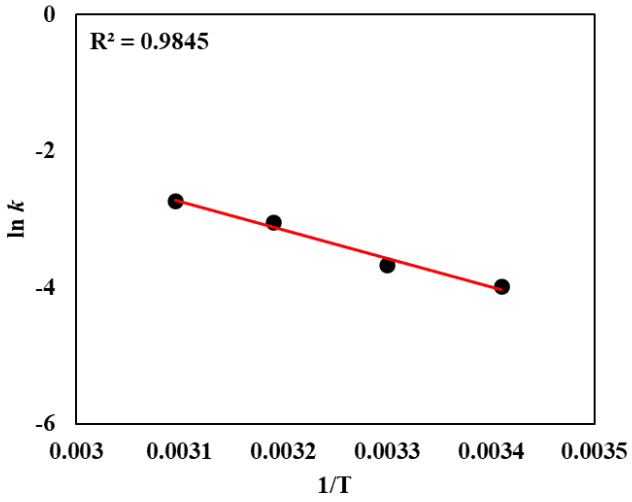

Figure 22 Plot of ln *k* Vs 1/T for glycerol acetalization

Furthermore, it is important to determine whether the rate of reaction is diffusion limited or is truly governed by the chemical step, where the catalyst is exploited to its maximum efficiency. It is reported in the literature that for the reactions following the diffusion regime, the activation energy is as low as 10-15 kJ/mol, while for the reactions governed by a truly chemical step, the activation energy is greater than 25 kJ/mol [58]. Here, for all the reactions the activation energies were found to exceed 25 kJ/mol, which indicates that all the reactions are governed by a true chemical step and none of it follows a diffusion regime.

It is noteworthy that amongst all the three transformations, the activation energy for esterification of levulinic acid was found to be the lowest (only 26 kJ/mol). This can be explained as follow.

Levulinic acid is a monocarboxylic keto acid, which requires only one acid group to convert into the desired ester, whereas succinic acid possesses two carboxylic acid groups, a diacid requiring a higher number of catalytic sites as well as prolonged reaction time to undergo diesterification reaction, to obtain the desired diester and the obtained activation energy is in good agreement with it.

Plausible mechanism

a) Esterification of levulinic acid with n-butanol

The plausible reaction mechanism for acid-catalysed esterification of levulinic acid is shown in Figure 23. Firstly, the adsorption of acid occurs on the surface of nMCM-48 and the protons present in SiW_{12} activate the carbonyl carbon of the carboxylic acid group, forming an electrophilic intermediate. Instantaneously, the nucleophilic attack of the hydroxyl group of alcohol occurs at the carbonyl carbon, forming an oxonium intermediate. This intermediate is stabilized by the negative charge generated on partially deprotonated SiW_{12}. At the expense of a proton back to the active site, the intermediate loses a water molecule and forms desired ester. In the overall process, the unique 3D cubic structure of nMCM-48 directs the reactant molecules to active catalytic sites by preventing the mass transfer limitations and stabilizes the deprotonated keggin structure. Whereas the anchored SiW_{12} provides sufficient catalytic sites for the activation of a carbonyl group and facilitates the attack of the nucleophile. Thus, the overall picture proposes that SiW_{12}/nMCM-48 generates a perfect synergy to carry out the esterification of levulinic acid.

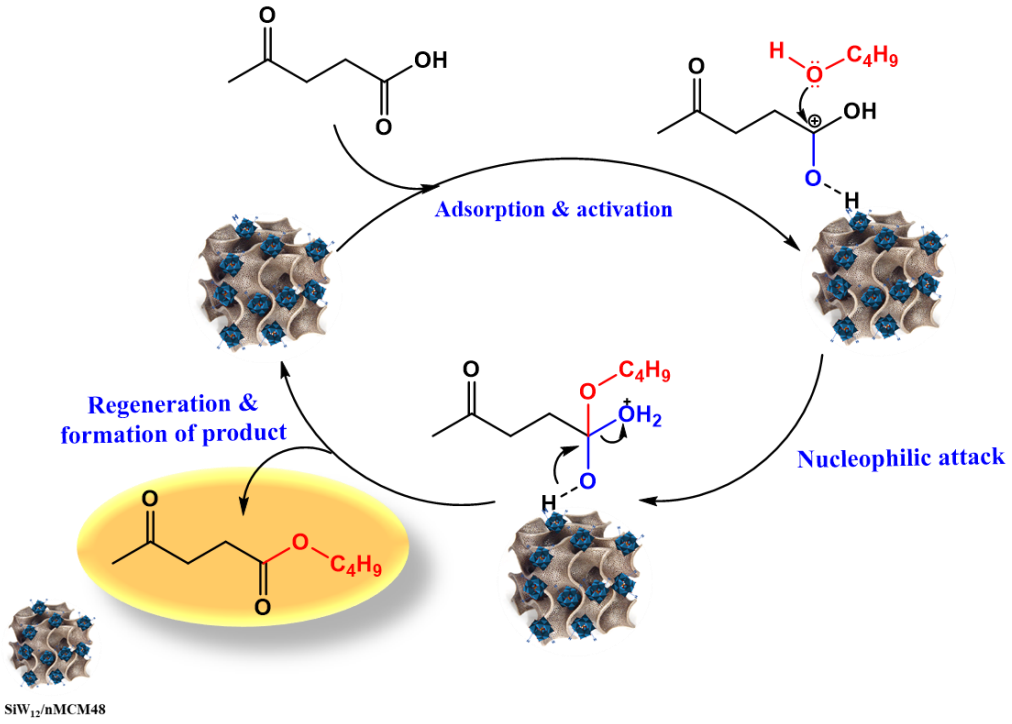

Figure 23 Plausible mechanism of esterification of levulinic acid with n-butanol over SiW_{12}/nMCM-48

b) Esterification of succinic acid with n-butanol

Undoubtedly, the acid catalysed esterification depends on the presence of acidic sites and the competitive adsorption of alcohol to that of a substrate (succinic acid). As shown in Figure 24, the succinic acid molecule first adsorbs on the catalyst, followed by the activation of carbonyl carbon by the Bronsted acid sites. A nucleophilic attack of a hydroxyl group of alcohol generates a tetrahedral intermediate which then loses a molecule of water and forms the monoester. The monoester undergoes the same pathway to give diester. However, the formation of the diester is competitive with that of the adsorption of alcohol. Henceforth, the Bronsted acidity of SiW_{12} promotes the second diesterification, giving the higher selectivity towards the diester. Here also, the cubic porous structure of nMCM-48 facilitates the ease of entry and exit of reactants and products, respectively. Thus, the higher acidity of SiW_{12} and pore network of nMCM-48 enables to achieve excellent conversion as well selectivity of the desired ester.

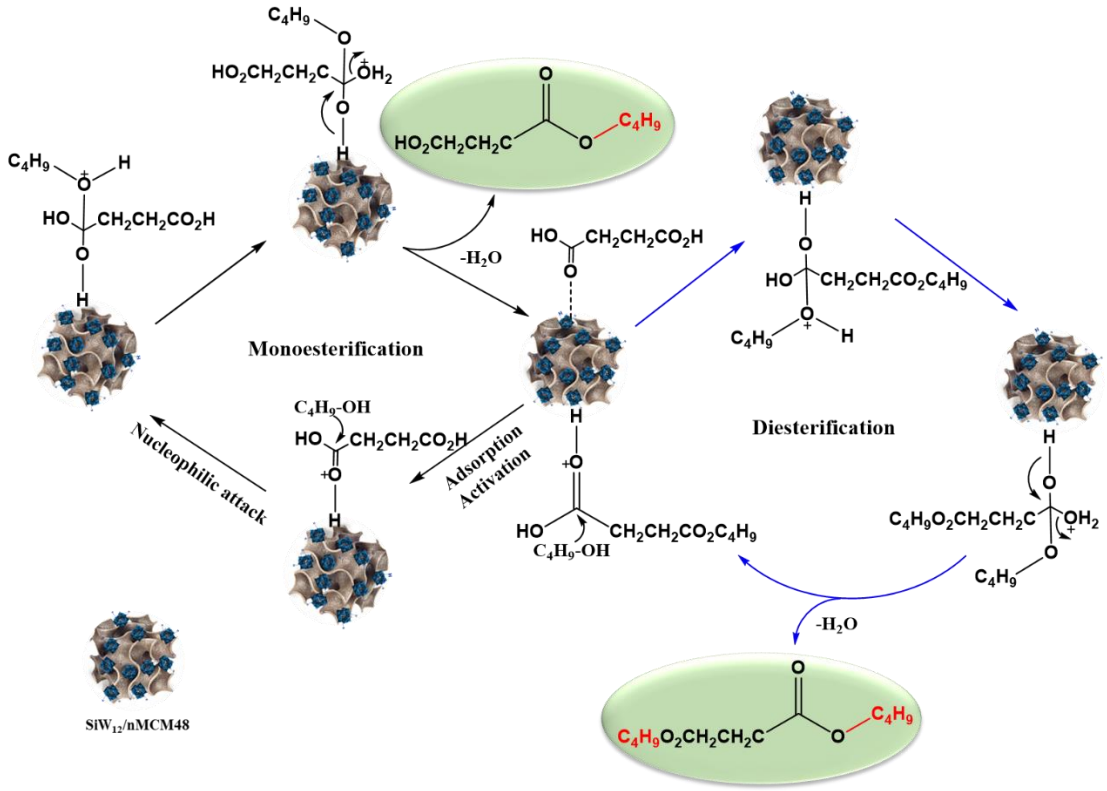

Figure 24 Plausible mechanism of esterification of succinic acid with n-butanol over SiW_{12}/nMCM-48

c) Acetalization of glycerol with furfural

For the acid-catalysed acetalization of glycerol with furfural, the first step is adsorption of furfural on the active catalytic site (Figure 25). The Bronsted acid sites present in SiW_{12} activate the carbonyl carbon of furfural, making it electrophilic. In the next step, the primary hydroxyl group of glycerol undergoes a nucleophilic attack on the carbonyl carbon and forms hemiacetal. Subsequently, depending on the orientation of the intermediate, either the primary or secondary hydroxyl group attacks the carbocation and the removal of the water molecule gives the cyclic acetals. In this case, the attack of another primary hydroxyl group of glycerol is dominant over the secondary one, thus giving the six-membered cyclic acetal, 1,3-dioxane as a major product.

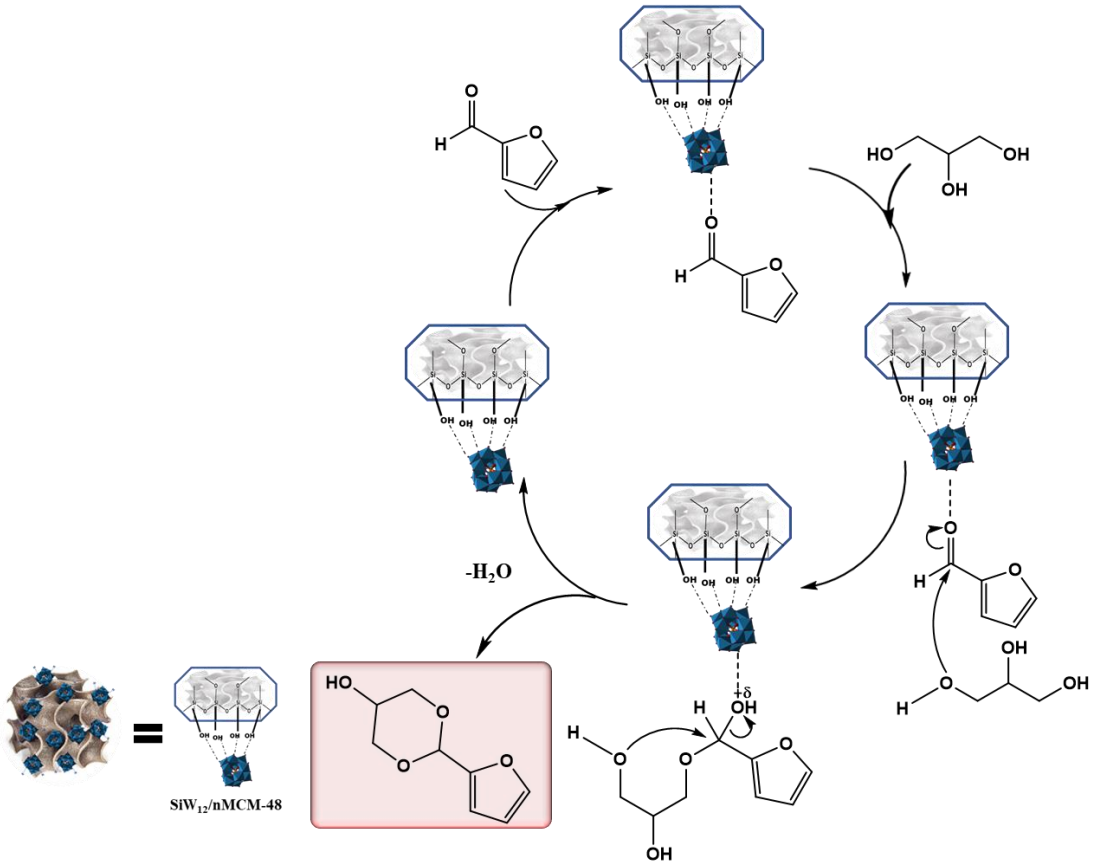

Figure 25 Plausible mechanism of acetalization of glycerol with furfural over SiW_{12}/nMCM-48

CONCLUSION

- First time, nano-porous MCM-48 was successfully synthesized by non-hydrothermal method and used as a support for anchoring parent silicotungstic acid (SiW_{12}). Powder XRD, Nitrogen adsorption-desorption isotherms and TEM confirms the 3D cubic geometry, nanoporosity and spherical morphology of nMCM-48, respectively. Furthermore, The BET surface area analysis depicts the successful filling of pores of nMCM-48 by SiW_{12} whereas the interaction between them was established by ^{29}Si MAS NMR.
- A probable representation of the interaction of SiW_{12} and nMCM-48 is shown in the adjoining figure,

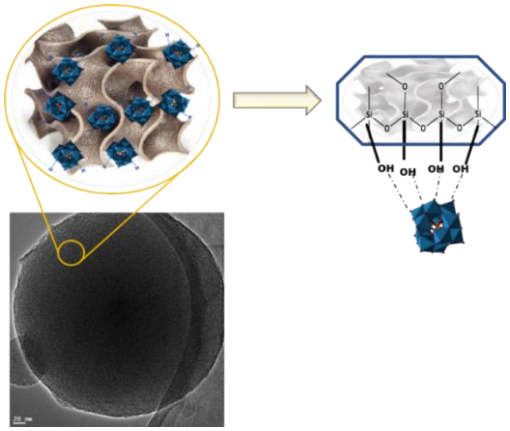

- The superiority of the catalyst lies in the outstanding activity at mild reaction conditions, for the synthesis of bio-fuel additives via catalytic esterification of levulinic acid and succinic acid (≥ 98% conversion) as well as acetalization of glycerol (89% conversion) with excellent TONs and TOFs.
- The activation energy order was found to be:

Levulinic acid esterification (26 kJ/mol) < **Glycerol acetalization (35 kJ/mol)** < **Succinic acid esterification (55 kJ/mol)**

- The plausible mechanism depicts that SiW_{12} significantly initiates the reactions while the 3D cubic geometry of nMCM-48 provides selectivity of the desired products.

REFERENCES

1. A. Patel, D. Morawala, H. Lankapati, B. Shah, and K. Maheria, Mater Today Proc (2021).

2. N. A. S. Ramli, N. I. Hisham, and N. A. S. Amin, Sains Malays 47, 1131 (2018).

3. F. Yang and J. Tang, ChemistrySelect 4, 1403 (2019).

4. A. F. Peixoto, M. M. A. Soliman, T. v Pinto, S. M. Silva, P. Costa, E. C. B. A. Alegria, and C. Freire, Biomass Bioenergy 145, 105936 (2021).

5. A. Najafi Chermahini and M. Nazeri, Fuel Process Technol 167, 442 (2017).

6. Z. Miao, Z. Li, J. Zhao, W. Si, J. Zhou, and S. Zhuo, Mol Catal 444, 10 (2018).

7. M. P. Pachamuthu, V. v Srinivasan, R. Karvembu, and R. Luque, Microporous Mesoporous Mater 287, 159 (2019).

8. E. Altuntepe, V. N. Emel'yanenko, M. Forster-Rotgers, G. Sadowski, S. P. Verevkin, and C. Held, Appl Microbiol Biotechnol 101, 7509 (2017).

9. L. Zhou, Y. He, L. Ma, Y. Jiang, Z. Huang, L. Yin, and J. Gao, Bioresour Technol 247, 568 (2018).

10. S. Zhou, D. Jiang, X. Liu, Y. Chen, and D. Yin, RSC Adv 8, 3657 (2018).

11. F.-F. Mao, W. Zhao, D.-J. Tao, and X. Liu, Catal Letters 150, 2709 (2020).

12. J. Yang, G. Li, L. Zhang, and S. Zhang, Catalysts 8, (2018).

13. A. V Nakhate and G. D. Yadav, ACS Sustain Chem Eng 4, 1963 (2016).

14. K. C. Maheria, J. Kozinski, and A. Dalai, Catal Letters 143, 1220 (2013).

15. K. Y. Nandiwale and V. v Bokade, Chem Eng Technol 38, 246 (2015).

16. W. Zhao, H. Ding, J. Zhu, X. Liu, Q. Xu, and D. Yin, J Bioresour Bioprod 5, 291 (2020).

17. F. G. Cirujano, A. Corma, and F. X. Llabrés i Xamena, Chem Eng Sci 124, 52 (2015).

18. M. A. Tejero, E. Ramírez, C. Fité, J. Tejero, and F. Cunill, Appl Catal A Gen 517, 56 (2016).

19. Q. Luan, L. Liu, S. Gong, J. Lu, X. Wang, and D. Lv, Process Saf Environ Prot 117, 341 (2018).

20. Y. Chen, X. Zhang, M. Dong, Y. Wu, G. Zheng, J. Huang, X. Guan, and X. Zheng, J Taiwan Inst Chem Eng 61, 147 (2016).

21. C. Delhomme, S. L. M. Goh, F. E. Kühn, and D. Weuster-Botz, J Mol Catal B Enzym 80, 39 (2012).

22. R. Fareghi-Alamdari, M. N. Niri, and H. Hazarkhani, J Chem Sci 130, 48 (2018).

23. C. Jing, L. Jinhua, D. Zhongxie, W. Yuehua, L. Zhen, J. Min, and R. Xiaoqian, Química Nova 41, 613 (2018).

24. A. Szelwicka, S. Boncel, S. Jurczyk, and A. Chrobok, Appl Catal A Gen 574, 41 (2019).

25. J. Hamdi, B. N. Diehl, K. Kilgore, S. A. Lomenzo, and M. L. Trudell, ACS Omega 4, 19437 (2019).

26. V. Brahmkhatri and A. Patel, Ind Eng Chem Res 50, 13693 (2011).

27. V. Brahmkhatri and A. Patel, Green Chem Lett Rev 5, 161 (2012).

28. V. Brahmkhatri and A. Patel, J Porous Mater 20, 209 (2013).

29. F. Adam, M. S. Batagarawa, K. M. Hello, and S. S. Al-Juaid, Chem Pap 66, 1048 (2012).

30. C. Gonzalez-Arellano, R. A. D. Arancon, and R. Luque, Green Chem 16, 4985 (2014).

31. C. Gonzalez-Arellano, S. De, and R. Luque, Catal Sci Technol 4, 4242 (2014).

32. E. Gutiérrez-Acebo, F. Guerrero-Ruiz, M. Centenero, J. S. Martínez, P. Salagre, and Y. Cesteros, Open Chem 16, 386 (2018).

33. R. R. Pawar, K. A. Gosai, A. S. Bhatt, S. Kumaresan, S. M. Lee, and H. C. Bajaj, RSC Adv 5, 83985 (2015).

34. A. Patil, S. Shinde, S. Kamble, and C. v. Rode, Energy Fuels 33, 7466 (2019).

35. B. Mallesham, P. Sudarsanam, G. Raju, and B. M. Reddy, Green Chem 15, 478 (2013).

36. B. Mallesham, P. Sudarsanam, and B. M. Reddy, Catal Sci Technol 4, 803 (2014).

37. J. R. Dodson, T. Avellar, J. Athayde, and C. J. A. Mota, Pure Appl Chem 86, 905 (2014).

38. S. K. Kundu, R. Singuru, T. Hayashi, Y. Hijikata, S. Irle, and J. Mondal, ChemistrySelect 2, 4705 (2017).

39. K. S. Arias, A. Garcia-Ortiz, M. J. Climent, A. Corma, and S. Iborra, ACS Sustain Chem Eng 6, 4239 (2018).

40. L. J. Konwar, A. Samikannu, P. Mäki-Arvela, D. Boström, and J.-P. Mikkola, Appl Catal B 220, 314 (2018).

41. C. A. Akinnawo, L. Mosia, O. A. Alimi, C. O. Oseghale, D. P. Fapojuwo, N. Bingwa, and R. Meijboom, Catal Commun 152, 106287 (2021).

42. J. N. Appaturi, R. Jothi Ramalingam, H. A. Al-Lohedan, F. Khoerunnisa, T. C. Ling, and E. P. Ng, Fuel 288, 119573 (2021).

43. M. Baithy, D. Mukherjee, A. Rangaswamy, and B. M. Reddy, Catal Letters 152, 1428 (2022).

44. M. M. Antunes, R. F. Mendes, F. A. A. Paz, and A. A. Valente, Catalysts 11, 1 (2021).

45. S. Singh and A. Patel, J Clean Prod 72, 46 (2014).

46. M. Thommes, K. Kaneko, A. v Neimark, J. P. Olivier, F. Rodriguez-Reinoso, J. Rouquerol, and K. S. W. Sing, Pure Appl Chem 87, 1051 (2015).

47. V. Zeleňák, D. Halamová, M. Almáši, L. Žid, A. Zeleňáková, and O. Kapusta, Appl Surf Sci 443, 525 (2018).

48. N. Narkhede and A. Patel, Appl Catal A Gen 515, 154 (2016).

49. Y. Zhang and S. Yang, J Wuhan Univ Technol Mater Mater Sci Ed 23, 346 (2008).

50. D. Bajuk-Bogdanović, I. Holclajtner-Antunović, M. Todorović, U. B. Mioč, and J. Zakrzewska, J Serbian Chem Soc 73, 197 (2008).

51. J. Xu, Z. Luan, H. He, W. Zhou, and L. Kevan, Chem Mater 10, 3690 (1998).

52. A. Sakthivel, K. Komura, and Y. Sugi, Ind Eng Chem Res 47, 2538 (2008).

53. D. Carriazo, C. Domingo, C. Martín, and V. Rives, J Solid State Chem 181, 2046 (2008).

54. V. Dellarocca, L. Marchese, M. L. Peña, F. Rey, A. Corma, and S. Coluccia, in Oxide-Based Systems at the Crossroads of Chemistry, edited by A. Gamba, C. Colella, and S. B. T.-S. in S. S. and C. Coluccia (Elsevier, 2001), pp. 209–220.

55. F. J. Berry, G. R. Derrick, and M. Mortimer, Polyhedron 68, 17 (2014).

56. K. C. Badgujar, V. C. Badgujar, and B. M. Bhanage, Fuel Process Technol 197, 106213 (2020).

57. A. Talebian-Kiakalaieh, N. A. S. Amin, N. Najaafi, and S. Tarighi, Front Chem 573 (2018).

58. G. C. (Geoffrey C. Bond, Heterogeneous Catalysis : Principles and Applications / G.C. Bond (Clarendon Press, Oxford [Oxfordshire] ; New York, 1987).